Measurement 229 (2024) 114405

Contents lists available at ScienceDirect

Measurement

journal homepage: www.elsevier.com/locate/measurement

The influence of the geographic positioning system error on the quality of ship magnetic signature reproduction based on measurements in sea conditions

J. Tarnawski [a,*], K. Buszman [b], M. Woloszyn [a], B. Puchalski [a]

[a] Faculty of Electrical and Control Engineering, Gdansk University of Technology, Gdansk, Poland
[b] Faculty of Navigation and Naval Weapons, Polish Naval Academy, Gdynia, Poland

ARTICLE INFO

Keywords:
Sea measurements
Magnetic variables measurement
Magnetic anomaly detection
Marine vehicles
Magnetic fields
Electromagnetic, modelling
Magnetic signatures
Model checking

ABSTRACT

In previous studies, the authors performed the magnetic signature reconstruction of the marine ship *Zodiak* as part of the measurement campaign focused on recording magnetic data and the relative position of a ship during its passage over a magnetometer immersed on the testing ground. A high degree of representation of the magnetic signature was obtained. However, the recorded measurement data revealed new patterns of the multi-dipole model behavior that were not observed in the synthetic data based analyzes. It was assumed that the main factor influencing the abovementioned behavior of the model is the error in determining the geographical position of the ship in relation to the magnetometer. Therefore, another research was carried out to determine the relative position of the ship and the measurement device in sea conditions, in the area of the test site used in the previous study. For this purpose, two different classes of GPS receivers were used. The first receiver was the same as that used to determine the position of *Zodiak* in the previous measurement campaign, while the second receiver, treated as a reference, was a top-class geodetic receiver. The difference in indications between these two receivers gave a picture of the scale of errors in the data recorded during the previous measurement campaign. These errors are used in the article to analyze the effect of inaccuracies in determining the ship position on the quality of magnetic signature reproduction. Two types of signature reproduction error were introduced – the error based only on the data collected from the ship's paths, and the error in the entire area of magnetic anomaly. The model of *Zodiak* was used to determine the value of the magnetic flux outside the paths. Profiles of differences in indications of GPS receivers at sea which were obtained from actual measurements were used to analyze the errors in determining the ship position. A measurable result of the work reported in the article is the map of the loss of quality of magnetic signature reproduction as a function of the ship position determination error, which can indicate the range of applicability of the model and the described method.

1. Introduction

The genesis of the measurements performed using the Furuno SC-50 GPS receiver to determine the geographical position accuracy [1] were the results of numerical modelling of magnetic signatures of *Zodiak* [2,3]. In order to determine the magnetic signature, underwater measurements were made of magnetic flux density of the ship moving along the cardinal directions at three different speeds [4]. The measurements allowed to create 12 curves of magnetic flux density changes for the x-, y- and z-components, and for the resultant magnetic flux density vector [5]. These results corresponded to the trajectories of the moving ship, determined on the basis of data recorded from the GPS receiver installed in the midship of *Zodiak*. The obtained changes in magnetic flux density values for each of the transitions were the input data for developing a multi-dipole model, which was then used to reconstruct the signature of a ship moving on an arbitrary course [5]. The comparison of the measured magnetic flux density with the results obtained from the numerical model showed discrepancies of up to 10 % of the maximum value of the resultant magnetic flux density vector. The accuracy of the magnetometers (Bartington Grad-03) used was specified by the manufacturer at +/- 1 nT, the same as sensor range ± 200 μT. The impact of such an error magnitude, (as well as 10 times and 100 times higher) was

* Corresponding author at: Gdansk University of Technology, Faculty of Electrical and Control Engineering, 11/12 Gabriela Narutowicza Street, 80-233 Gdansk, Poland.
E-mail address: jaroslaw.tarnawski@pg.edu.pl (J. Tarnawski).

https://doi.org/10.1016/j.measurement.2024.114405
Received 19 September 2023; Received in revised form 14 February 2024; Accepted 26 February 2024
Available online 1 March 2024

analyzed in [6], and it was found that a 1 nT signature determination error had a marginal effect on the signature value. Therefore, it seemed reasonable to assume that there are other sources of error in the signatures presented in [5] than the magnetometer error, and that these errors refer to the position determination of the ship and the measuring device.

The main possible source of inaccuracy in reconstructing the ship's magnetic signature is the inaccuracy in determining the geographical position of the ship. This inaccuracy results from the operation of a typical satellite navigation system which determines a pseudo-distance between the receiver and individual satellites on the basis of measuring the delay of signals reaching the receiver [7,8]. The issue of inaccuracy of geographic positioning in navigation is discussed in [9,10,11], among other works. It is noteworthy here that when analysing it, the duration of the conducted measurements should also be taken into account, as was demonstrated in [12]. The accuracy in determining magnetic signatures is important in many areas, such as classifying units, estimating the risk of crossing dangerous waters, or minimizing the signature [37,38].

In [5], the *Zodiak* signatures were determined based on the relative position of the measuring device and the moving ship, the ship's heading values, and the magnetic flux density values recorded by the measuring device during ship motion.

In order to determine the degree of influence of the navigation data on the quality of the determined numerical multi-dipole ship model, it was decided to carry out additional measurements of the accuracy of the GPS receiver used during the 2019 survey by comparing its recordings with those simultaneously obtained from a geodetic reference receiver.

The general relation for determining the magnetic signature of a ship can be written as:

$$(MFD_{Bx}, MFD_{By,} MFD_{Bz}) = \mathrm{f}(xMD, yMD, zMD, xShip, yShip, headingShip, B_x, B_y, B_z) \quad (1)$$

where:$MFD_{Bx}, MFD_{By,}\ MFD_{Bz}$– the determined x, y, z components of the magnetic field, respectively (anywhere at the measurement depth and below),$xMD,\ yMD, zMD$ – geographical location coordinates of the measuring device,$xShip, yShip$– geographical location coordinates of the ship,$headingShip$– geographical direction of the ship,$B_x,\ B_y,\ B_z$– the values of the magnetic field components measured by the magnetometers (only along the ship's passage route).

Analyzing (1), we must note that the measurement uncertainty is characterized by the stationary position of the measuring device and its possible geographical position variations in depends on GPS almanac during several hours of the measurement campaign, represented by $xMD,\ yMD, zMD$. The uncertainty in the measurement also applies to $xShip, yShip, headingShip$ which in the signature calculations is represented by 12 ship passages (in 4 directions N, E, S, W with 3 different speeds 5, 7, 10 kn). Measurement uncertainty is also introduced by magnetometers providing information on the components of the magnetic field B_x, B_y, B_z. According to the manufacturer of measuring devices, this error does not exceed 1 nT. Analyzes of the impact of this type of error on signatures were carried out in [6] and as their impact is negligible compared to position determination errors, these errors are not analyzed in this paper, i.e. the measured values are considered as reference. The ship's heading is also assumed to be determined without error.

The number of data related to determining the ship's position in relation to the measuring device that influence the form of signatures is very large, the relationship between these quantities is strongly nonlinear, form of the relationship between these quantities and the asymmetric, irregular error distributions make it pointless to consider this influence in a deterministic or analytical way.

The authors do not have a precise analytical relationship (1) between the error in determining geographical position and its impact on signatures. Instead, a two-step approach is proposed. In the first stage, the parameters of the multi-dipole model are determined based on measurement data using optimization (see section 4.4). In the second stage, the model is used to determine signatures (chapter 3). The proposed approach does not analyze the influence of a single quantity on signatures in the style of sensitivity analysis. This article proposes an approach presented in [39,40] where uncertainty evaluation is performed using the propagation of distributions. The distributions of errors in determining the position, both stationary and during ship passages, are introduced into Monte Carlo simulations and thus ranges of potential forms of magnetic signatures are obtained. Symbolically, the situation is presented in Fig. 1. there are the distributions of the position of the stationary measuring device and the dynamic passages of the ship, inside there is a relation linking these quantities, on the right we get the distributions of signatures.

A similar issue discussed in this paper related to positioning uncertainty and uncertainty in magnetic measurements was presented by the authors [41]. The method described by the authors [41] involves studying the kinematics of the positioner using a many-body system approach. The authors included geometric errors of the manipulator in the mathematical model using a homogeneous transformation matrix to numerically estimate the positioning uncertainty of the positioner. The positioning uncertainty authors combined with the magnetic measurement uncertainty using the magnetic field gradient as a sensitivity coefficient. In paper [42], the authors analyze the source of EM radiation (PCB) based on the measured field in a plane parallel to the plane in which the printed circuit board is located, z0 distant from the source. The presented method of synthesizing a model of a multi-dipole EM radiation source, such as a PCB, uses data recorded from the entire measurement matrix. This is possible due to the stationary nature of the experiment. A study was carried out on the variable EM radiation from a PCB in the range of several hundred MHz to several GHz. In an article related to the ship's measurements, the authors conducted an analysis of changes in the constant component of the magnetic field. The differences presented indicate the possibilities of a wide range of methods used for inversion modeling of various sources of disturbance of local magnetic, electric or EM fields in the context of electromagnetic compatibility. In both cited papers, there are similarities in the approach, the use of a multi-dipole model, and inverse modeling, but the main difference is that the aim of the authors of these publications is to build and verify a model of the phenomenon. For this purpose, theoretical approaches and disturbance models in the form of normal distributions are used in [41]. In [42] a position-stationary and time-dependent approach is presented. This paper considers the impact of measured errors in determining geographical position on the value of magnetic signatures.

The objectives of the paper are:

- development of a comprehensive, coherent approach to analyzing the error in determining the geographical position on the quality of magnetic signatures, taking into account the passages of ship in different directions,
- conducting an analysis of the impact of the error in determining the position of the Zodiak ship on the developed signatures.

Original contribution contains:

- determining potential errors affecting the quality of signature reproduction, uncertainty budget approach,
- planning and executing a measurement campaign to determine the nature of the errors of a classic GPS receiver and their ranges,
- development of error distributions and their analysis,
- implementation of the ship's passage according to a given schedule according to the Metropolis-Hastings algorithm with an error profile imposed,
- planning and conducting a Monte Carlo analysis integrating all potential errors affecting the signatures,

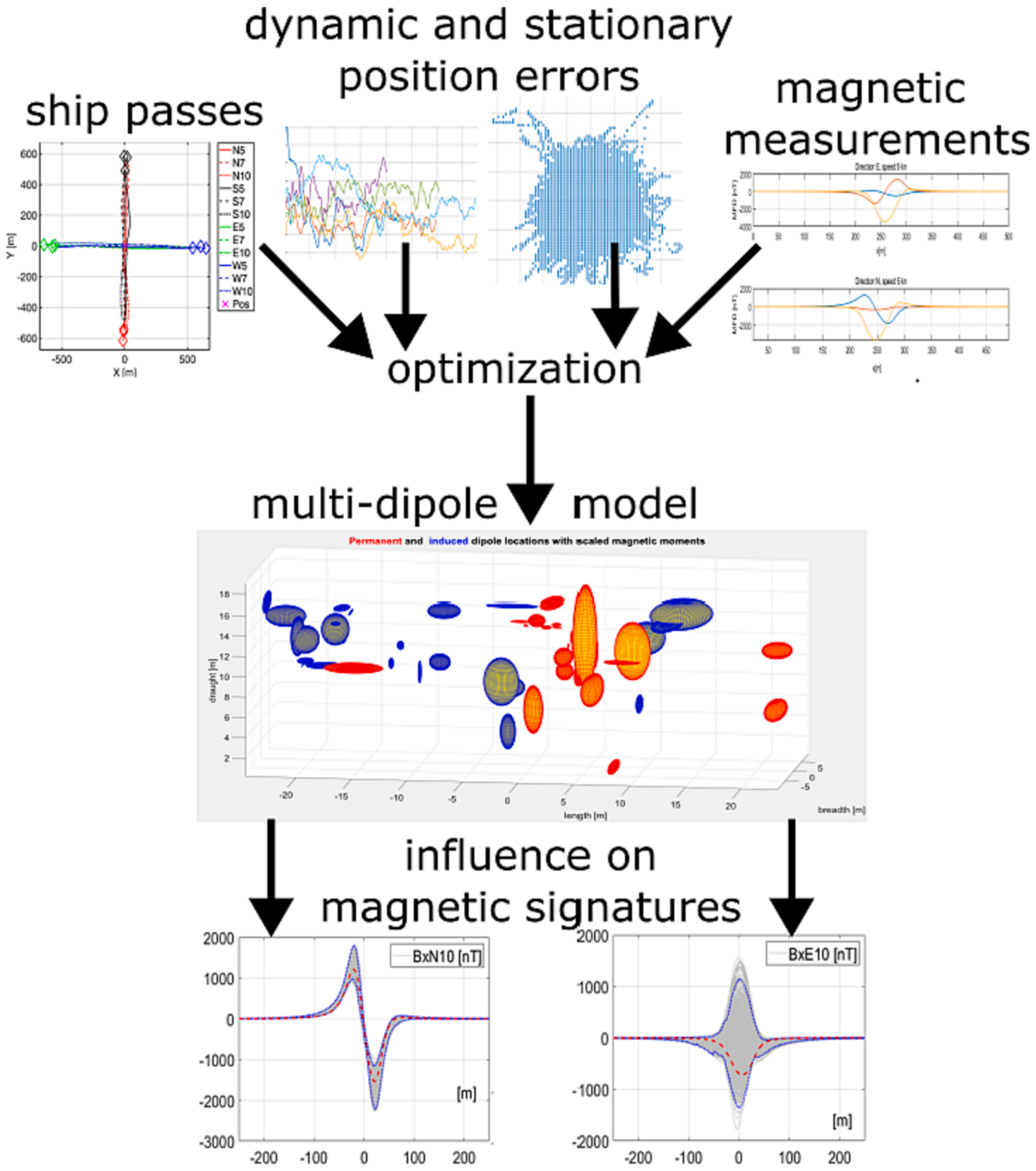

Fig. 1. Evaluation of position measurement uncertainty.

- presenting the impact of errors on the quality of signatures in qualitative and quantitative form,
- determining with a specific confidence interval in which intervals the original signatures of the Zodiak ship could have been located.
- The innovations of the paper are:
- the authors have performed innovative work because they have not found such an analysis of such a scale and nature in the scientific literature,
- the authors have developed a system for analyzing the impact in determining the position on the quality of signatures, taking into account data from various paths (PKS) and various directions,

- unlike most studies, the analysis took into account actual data (measured by the authors) on error distributions.

2. Measurement campaign

The idea of the representation of the local magnetic field disturbance (magnetic signature of the ship) obtained from the measurements performed on a moving ship is shown in Fig. 2. The measured object was the marine ship *Zodiak* moving at a given course and speed. The local magnetic field disturbance was measured using a triaxial magnetometer located at a specified geographical position and depth. The data samples were recorded at times resulting from the sampling frequency of the A/D converter in accordance with Fig. 3. At the same times, the geographical position of the moving ship was also recorded by the navigation system, the diagram of which is shown in Fig. 4. The instantaneous geographical position of the ship was adjusted to the XY plane, for which the axes were expressed in metres, taking into account the speed of the ship. The values of the recorded magnetic flux density components were assigned to respective geographical positions of the ship expressed as a distance [m] based on the GPS time. The result of the described measurement method for one passage is the magnetic flux density disturbance curve, for which the first sample corresponds to the area in front of the ship and the last sample to the area behind the ship. The course of the magnetic flux density disturbance changes as a function of the distance where its smallest value corresponds to the extreme left position of the axis (ship's bow space) means that the ship's bow is on the left side with respect to the stern. The results of the measurement, complemented with the actual ship's position in relation to the individual components of magnetic flux density for the dynamic measurement, are shown in Fig. 2.

When considering dynamic ship measurements, the area of concern is described by the latitude and longitude of the recorded trajectory. Using the Matlab environment, a conversion was carried out from angular values to distances expressed in metres relative to the centre of the Cartesian coordinate system in which the underwater measurement module was located. The obtained result had the form of a pair of vectors x and y, where x is associated with longitude E and y with latitude N, as shown in Fig. 5. The triaxial magnetometer used in the measurements recorded individual components of the magnetic flux density shown in Fig. 5. When unifying the x- and y-coordinates and the B_x and B_y components, the following relationships were assumed:

- the B_x component determines the direction of the OY axis, i.e., positive y values,
- the B_y component determines the direction of the -OX axis, i.e., negative x values.

Additionally, taking into account the assumption adopted in Fig. 2 that the beginning of the disturbance curve concerns the bow part and its end the stern part of the vessel, the vessel position should be rotated with respect to the z-axis for the x and y coordinates to take the opposite values "-y" and "x" considering the directions of the magnetic flux density components B_x and B_y.

The accuracy of the Furuno SC-50 GPS receiver was measured using a reference RTK (Real Time Kinematic) geodetic receiver [14,15], which was a Leica GS18T [16], together with a CS20 controller [17]. The geographic position of the reference receiver was determined using the corrections received from the nearest SmartNet reference stations (Fig. 6) [18], via GPRS (General Packet Radio Service) packet transmission in the RTCM (Radio Technical Commission for Maritime) standard.

The accuracy of determining the geographical position of the reference system was 1 cm [19]. This result made it possible to determine the errors of the tested GPS receiver using the comparative method. The position determination accuracy of the Furuno SC-50 system was 10 m for the GPS standard, 5 m for DGPS (Differential Global Positioning System) corrections [20,21], and 3 m for EGNOS (European Geostationary Navigation Overlay Service) corrections [22,23].

2.1. Measurements in static mode

The static mode measurements were made using the DGPS and GPS-RTK receivers described earlier. The satellite navigation system Furuno had the same configuration as Zodiak onboard measurements (see Fig. 4). The antenna of the DGPS Furuno receiver was placed on the roof of the Naval Academy building, at an absolute height of 18 m. This antenna position was recorded with the reference receiver, i.e., Leica GPS-RTK, continuously for 3 days with a time interval of 1 s.

The horizontal distance between the position of the antenna situated on the roof of the building (Pos. 2) and that of the underwater measurement system (Pos. 1) [5] was 4720.1 m (Fig. 7).

Based on the data recorded by the Furuno GPS receiver, the distribution of the distance between the recorded position and the actual geographic position obtained from the reference receiver was determined (Fig. 8, Fig. 9). The average position error did not exceed 1.2 m, while the maximum error reached 7.3 m (Fig. 10).

In addition to the geographic position, other parameters were recorded, of which the number of satellites and GPS fix are presented in Fig. 10. The number of satellites oscillated between 6 and 12 throughout the measurement, while for most of the time (more than 99 %) the GPS fix was 1 (GPS correction, for which the accuracy is +/-12 m).

2.2. Measurements in dynamic mode

The dynamic mode measurements were carried out in the area of *Zodiak* operation. The trajectories with velocities analogous to those recorded during previous *Zodiak* measurements were taken into account. The graphical measurement plan is shown in Fig. 11 and the actual location of the measurement area is shown in Fig. 12 [5].

2.3. Description of GPS receiver accuracy measurements

The accuracy of the GPS receiver was measured using a hybrid boat (RIB) with two measuring systems: the test system and the reference system, installed in the bow (Fig. 13). The distance between the antenna centres of the Furuno GPS receiver (test system) and the Leica receiver (reference system) was 0.66 m. This relative position of the antennas

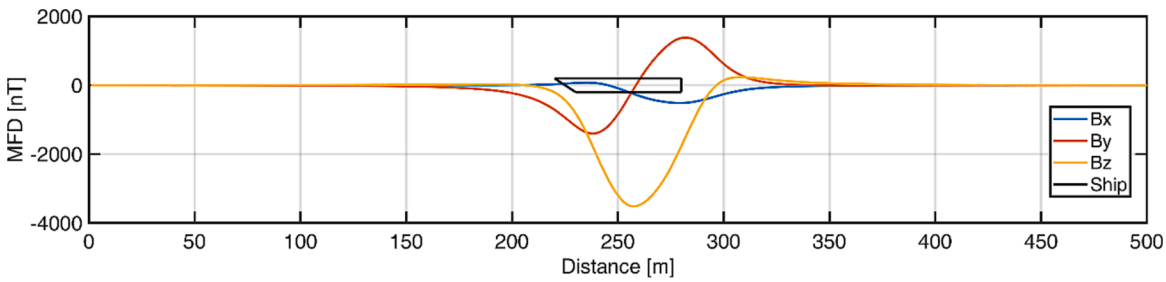

Fig. 2. Curves of measured magnetic flux density components with superimposed vessel shape.

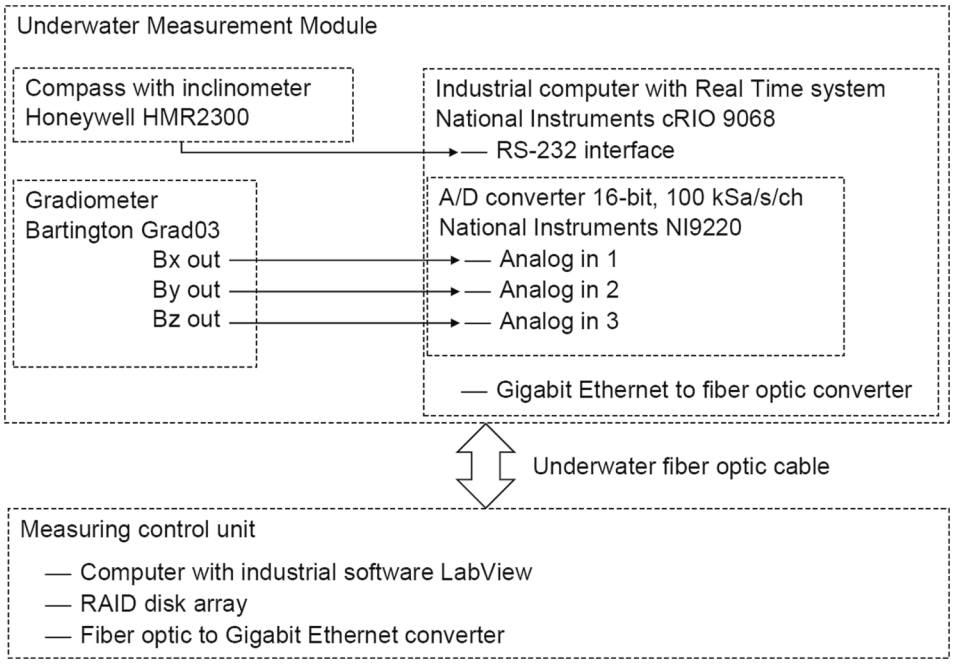

Fig. 3. Diagram of Underwater Measurement Module components.

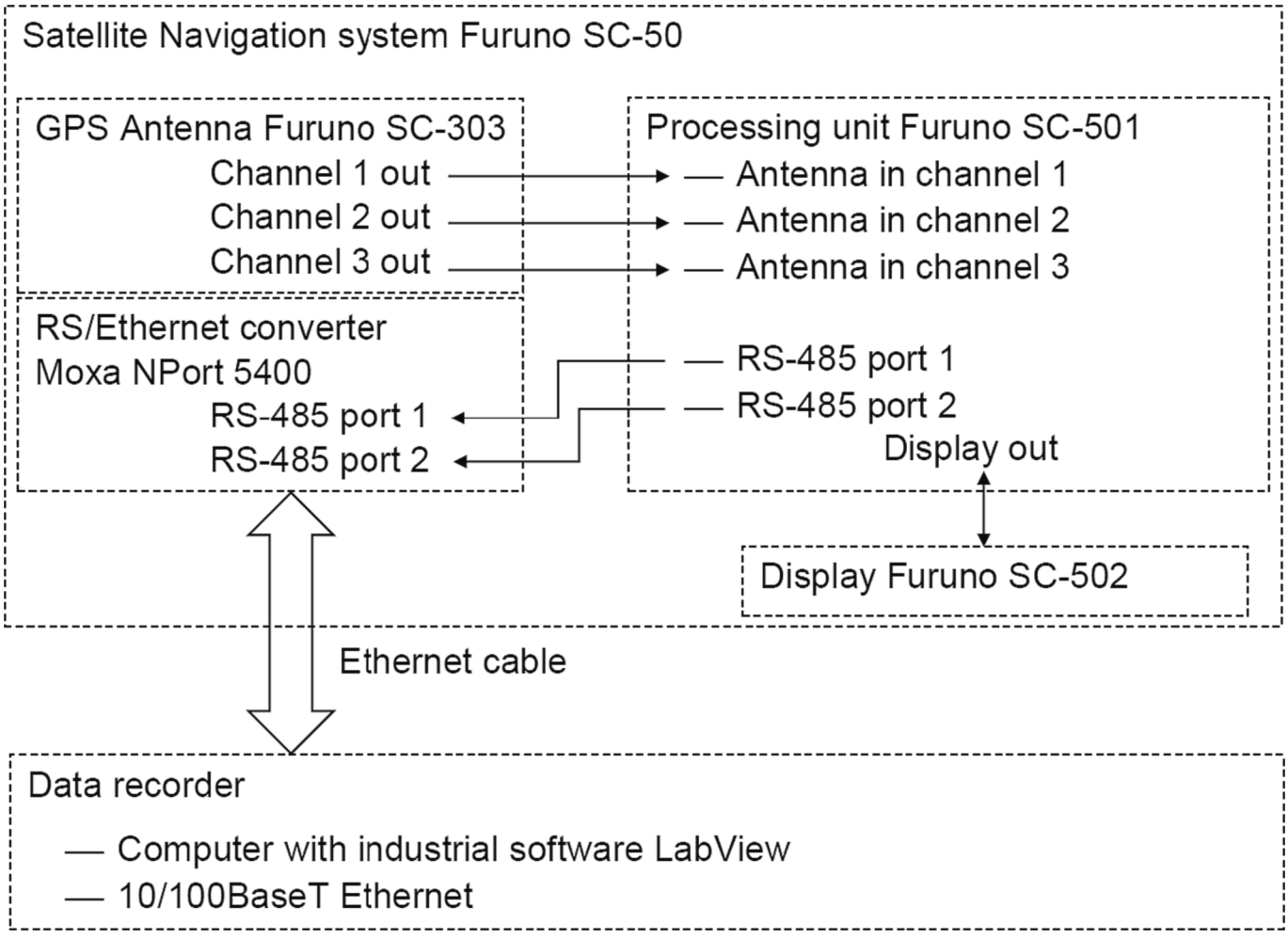

Fig. 4. Diagram of onboard satellite navigation system components.

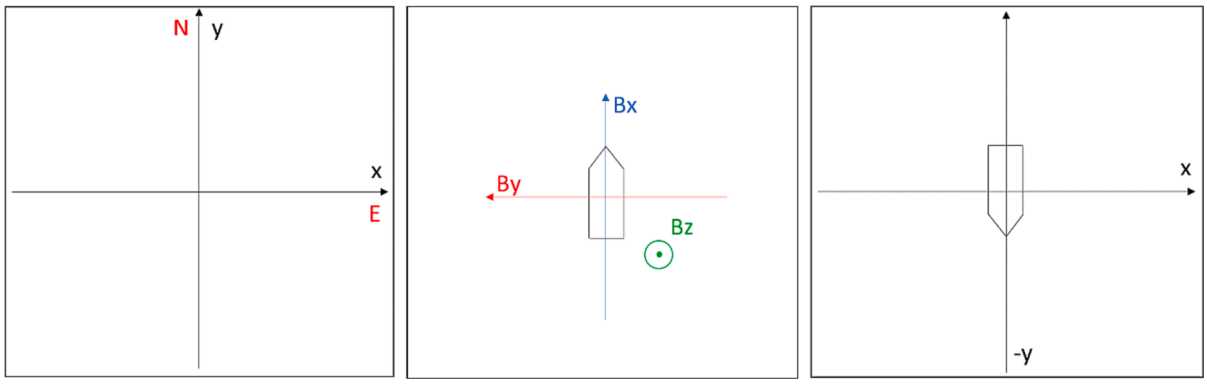

Fig. 5. Coordinate transformation (left: result of coordinate conversion from Matlab; center: directions of magnetic flux density components; right: coordinates considering ship motion).

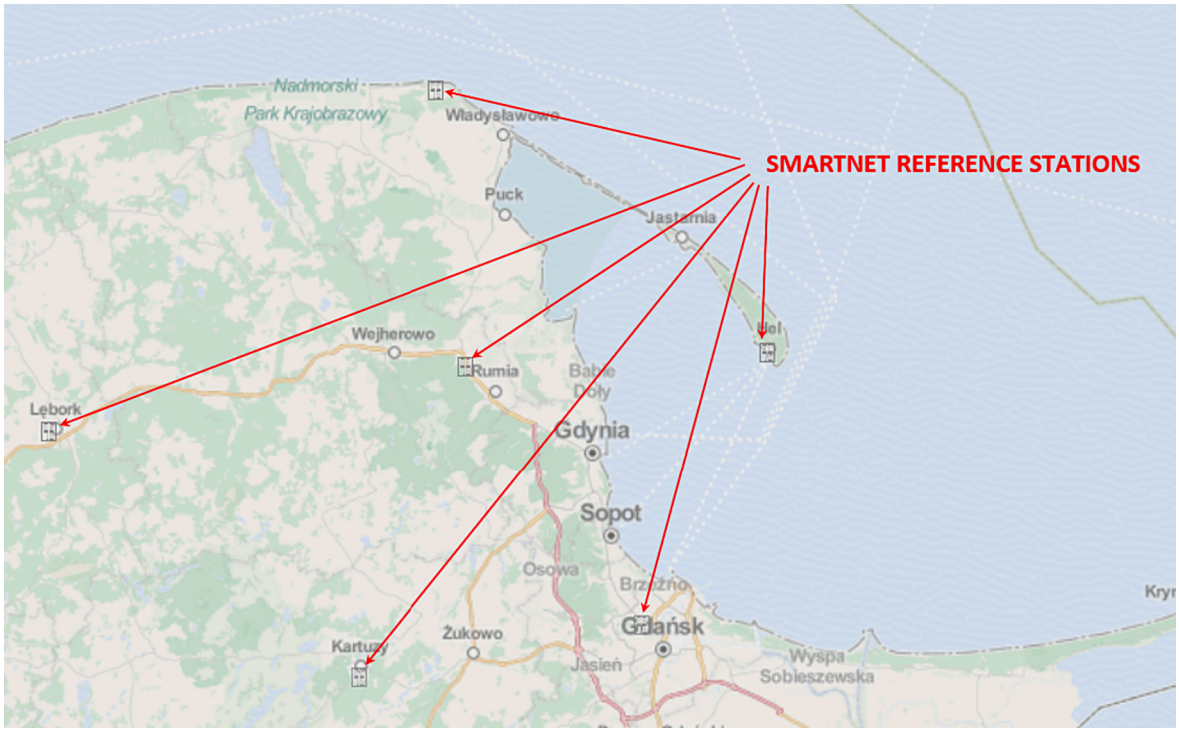

Fig. 6. Distribution map of SmartNet reference stations in the Gulf of Gdansk. [16].

was taken into account in the data processing to correct the position of the Furuno GPS antenna to that of the reference system antenna.

During each measurement, the hybrid boat moved at the set speed and course following the motion parameters of *Zodiak* in the previous measurement campaign. A photo of the on-board navigation system of the hybrid boat is shown in Fig. 14.

The recorded trajectories corresponded to the area where the *Zodiak* measurements were carried out in the previous measurement campaign. The central point of the measurements was the geographical position of the underwater measuring module, in relation to which the limiting positions for each of the cardinal directions were determined. This point was the same for the past *Zodiak* measurements and for the present GPS receiver accuracy measurements making use of a reference geodetic receiver. The resulting GPS tracks converted to a metric coordinate system for both *Zodiak* and the hybrid boat are shown in Fig. 15.

The obtained trajectories of the hybrid boat are described as follows: the letter N, S, E, W denotes the direction of motion of the vessel (*Zodiak* or hybrid boat), while the numerical value (5, 7, 10) denotes its assumed speed. The basic motion parameters of *Zodiak* and the hybrid boat after the conducted measurements are summarised in Table 1. The assumed and actual values of speed and the shortest distance from the position of the underwater measuring module (CPA - Closest Point of Approach) are given.

The recorded motion trajectories of the hybrid boat are presented in the XY plane in the metric scale. The coordinates (0,0) denote the position of the measurement module. The GPS tracks of the reference receiver and the tested receiver were plotted together in the joint diagrams taking into account the offset between the antenna centres. The tracks recorded by the two receivers are shown in Fig. 16 and Fig. 18, while the corresponding differences between them are shown in Fig. 17 and Fig. 19.

Based on the recorded GPS tracks of the vessel, the average position error was analysed taking into account all samples from the two satellite navigation systems. The analysis was performed independently for each passage of the vessel. Then, the mean error (MAE) and the root mean square error (RMSE) of determining the position by the tested system in relation to the reference system were calculated. Moreover, the difference between the mean and the root mean square error for each

Fig. 7. Satellite images with marking of survey positions for static mode (Pos.2) and dynamic mode (Pos. 1) measurements, and a photo of the Furuno GPS antenna placed on the roof together with the antenna of the Leica GPS-RTK reference receiver.

transition was calculated. The results obtained are shown in Fig. 20.

Analysing the obtained values of the geographic positioning errors, the lowest error is characteristic for the transitions at the lowest speed, i. e. 5 kn, and in this case the position error oscillates about 5 m. The error values increase with the increasing speed, and for 7 kn they are in the range of 7—8 m. For the highest speed, i.e., 10 kn, the errors exceed 10 m, reaching the highest value of 12 m for transition N10.

2.4. Background magnetic flux density fluctuations

Based on the results of real conditions measurements carried out for the Zodiak ship, the local background magnetic flux density fluctuations were analysed [5]. The fluctuations over a short time interval (30 s) had reached ± 1.5 nT for each axis. The results obtained from the entire measurement campaign, during a period of 7 h, were also analysed, for which the fluctuations for the x, y and z components reached 72 nT, 36 nT and 114 nT, respectively. The background mean values for this measurement location for the x, y and z components were 16,081 nT, 823 nT and 45,944 nT, respectively. The measured vessel magnetic flux density values ranged from −2000 to 2000 nT for B_x,

−1800 to 1800 nT for B_y and −4000 to 1000 nT for B_z. During the measurements, the current value of the individual components of the earth's magnetic flux density was subtracted from the measured signals. In this approach, the influence of slow changes in the earth's field was minimised. The magnetic noise values were 1,000 times smaller than the measured values of the ship's signatures. The resolution and sensitivity of the measuring equipment was sufficient without affecting the analysis results. In view of the abovementioned, the influence of the accuracy, resolution of the magnetometer and the noise analysed is negligible.

3. The multi-dipole model

The detailed form of the multi-dipole model based on [5] is given by (2) ÷ (4)

$$\mathbf{B} = \sum_{i=1}^{m+n} \mathbf{B}_i(\mathbf{M}_i, \mathbf{R}_i) = \sum_{i=1}^{m+n} \frac{\mu_0}{4\pi} \cdot \left(\mathbf{R}_i^T \mathbf{M}_i \mathbf{R}_i \cdot \frac{3}{\boldsymbol{R}_i^5} - \frac{\mathbf{M}_i}{\boldsymbol{R}_i^2} \right) \tag{2}$$

$$\mathbf{B} = \begin{bmatrix} B_x \\ B_y \\ B_z \end{bmatrix}, \mathbf{B}_i = \begin{bmatrix} B_{x,i} \\ B_{y,i} \\ B_{z,i} \end{bmatrix}, \ \mathrm{M}_i = \begin{bmatrix} m_{x,i} \\ m_{y,i} \\ m_{z,i} \end{bmatrix}, \ \mathrm{R}_i = \begin{bmatrix} (x - x_i) \\ (y - y_i) \\ (z - z_i) \end{bmatrix}, \tag{3}$$

$$R_i = |\mathbf{R}_i| = \sqrt{(x - x_i)^2 + (y - y_i)^2 + (z - z_i)^2} \tag{4}$$

where $\mathbf{B}$ is the magnetic flux density vector; $\mathbf{B}_i$ is the magnetic flux density vector of i-th magnetic dipole, where $i = 1, \ldots, m, m + 1, \ldots, m+n$; m is the number of permanent dipoles; n denotes the number of induced dipoles; $\mathbf{M}_i$ is the vector moment of i-th magnetic dipole in each orthogonal direction (x, y, z); $\mathbf{R}_i$ denotes the distance vector of the analysed point (x, y, z) from the i-th dipole with coordinates (x_i, y_i, z_i) along (x, y, z) directions; $\mathrm{R}_i = |\mathbf{R}_i|$ denotes the distance, as the vector length, between two points (x, y, z) and (x_i, y_i, z_i), and $\mu_0 = 4\pi 10^{-7} H/m$ is the absolute magnetic permeability of space. Note that the magnetic moments of the dipoles $m_{x,i}, m_{y,i}, m_{z,i}$ can have permanent $m_{xP,i}, m_{yP,i}, m_{zP,i}$ (P) or induced nature $m_{I1,i}, m_{I2,i}, m_{I3,i}$ (I) (see [5,6,13] for details).

For different ship's headings ϕ, the positions x_i, y_i and magnetic

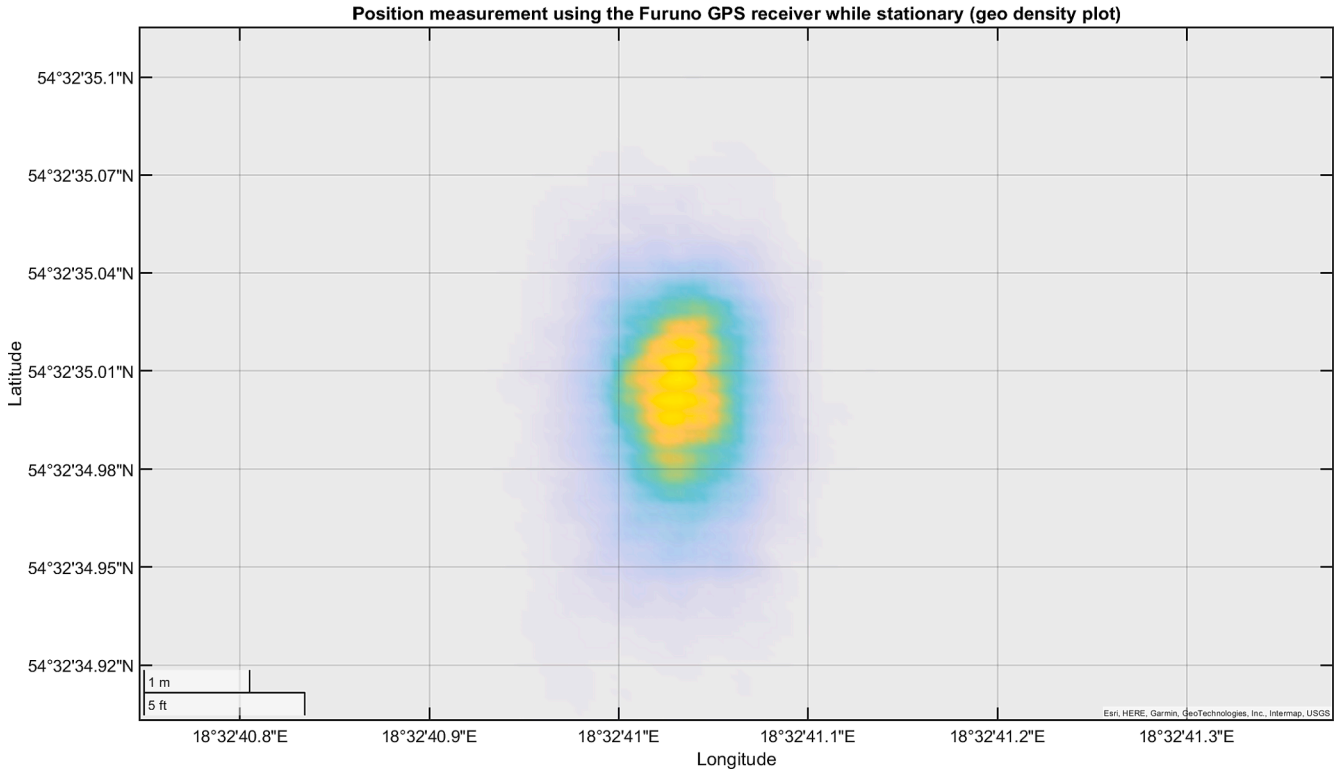

Fig. 8. Geo density plot for stationary Furuno receiver.

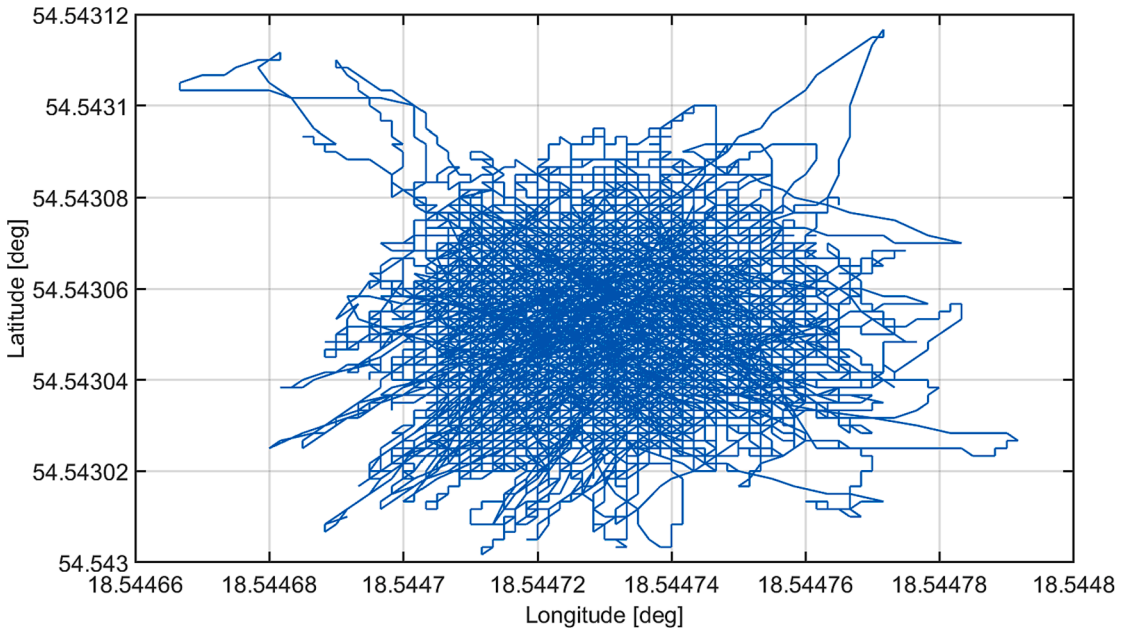

Fig. 9. Spread of geographic position data recorded with Furuno GPS receiver placed on the roof of the building.

moments $m_{x,i}, m_{y,i}$ of each dipole should be recalculated.

Transformed version of dipole coordinates denoted $\mathbf{R}'_i$ is given by equations (5)-(6)

$$x'_i = x_i \cdot cos(\phi) - y_i \cdot sin(\phi) \tag{5}$$

$$y'_i = x_i \cdot sin(\phi) + y_i \cdot cos(\phi) \tag{6}$$

where: ϕ is the object's heading, and x'_i and y'_i denote the transformed coordinates of the i-th dipole location.

A more complicated situation concerns the transformation of magnetic moments because there are different formulas for induced moments and others for permanent ones.

For $i = 1, \ldots, m$

$$\mathbf{M}'_i = \begin{bmatrix} m'_{x,i} \\ m'_{y,i} \\ m'_{z,i} \end{bmatrix} = \begin{bmatrix} m_{xP,i} \cdot cos(\phi) - m_{yP,i} \cdot sin(\phi) \\ m_{xP,i} \cdot sin(\phi) + m_{yP,i} \cdot cos(\phi) \\ m_{zP,i} \end{bmatrix} \tag{7}$$

where: $m'_{x,i}$, $m'_{y,i}$, $m'_{z,i}$ denote the transformed permanent magnetic

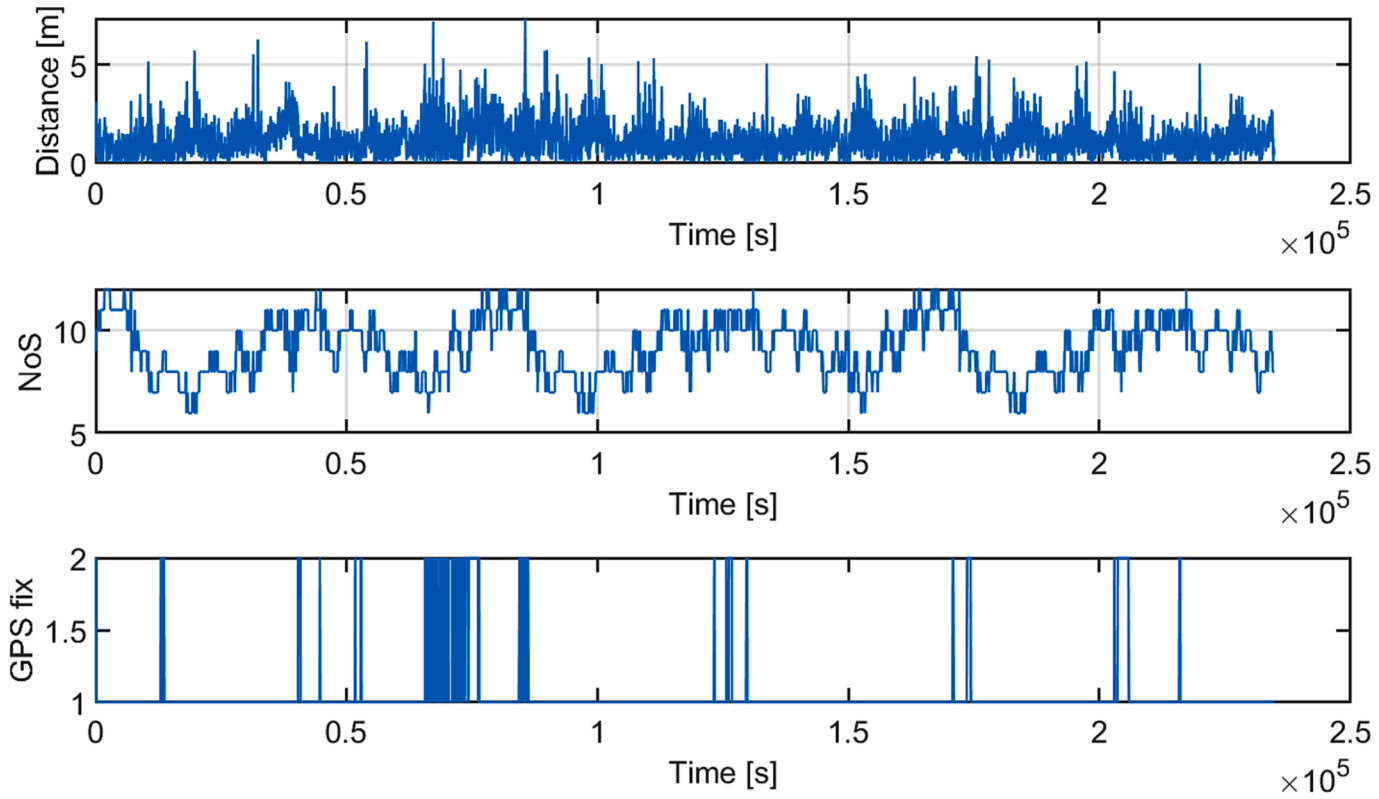

Fig. 10. Distance error between positions read from the reference receiver and the Furuno receiver (top), number of satellites (middle), and GPS fix parameter (bottom, 1 - GPS correction, 2 - DGPS correction [[24]]).

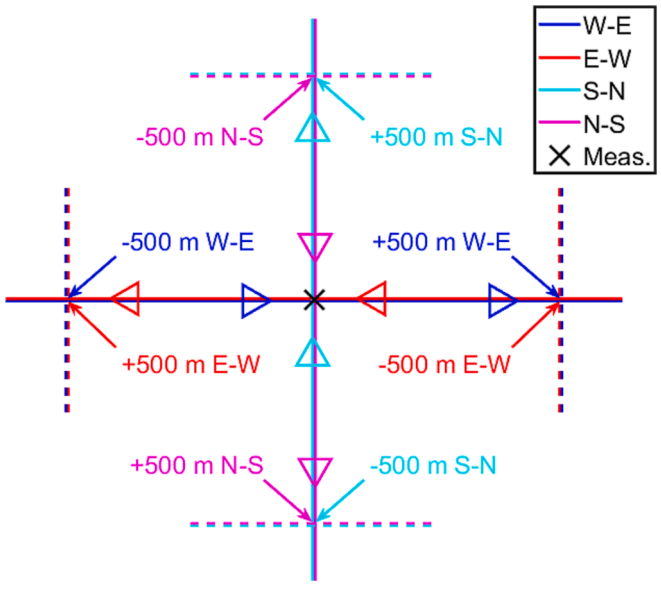

Fig. 11. Schematic diagram of trajectories for which GPS accuracy measurements were carried out.

moments of i-th permanent dipole, and $m_{xP,i}$, $m_{yP,i}$, $m_{zP,i}$ denote the components of permanent magnetic dipole moments calculated for $\phi = 0°$ in orthogonal (x, y, z) directions before transformation.

For $i = m+1, \ldots, m+n$

$$\mathbf{M}'_i = \begin{bmatrix} m'_{x,i} \\ m'_{y,i} \\ m'_{z,i} \end{bmatrix} = \begin{bmatrix} m_{I1,i} + m_{I2,i} \cdot cos^2(\phi) \\ m_{I2,i} \cdot sin(\phi) \cdot cos(\phi) \\ m_{I3,i} \end{bmatrix} \quad (8)$$

where: $m'_{x,i}$, $m'_{y,i}$, $m'_{z,i}$ denote the transformed induced magnetic moments of i-th induced dipole, and $m_{I1,i}, m_{I2,i}, m_{I3,i}$ denote the components of induced magnetic dipole moments calculated for $\phi = 0°$ in orthogonal (x, y, z) directions before transformation.

Dipole locations and dipole magnetic moments (both permanent and induced) are determined using the optimization process using as reference data from four ship headings (N° $\phi = 0^\circ$, W $\phi = 90^\circ$, S $\phi = 180^\circ$, E $\phi = 270^\circ$). A curve fitting method was applied to find the model parameters in order to reproduce the magnetic signature as close as possible (in a least squares sense) to the measured values. The model parameters are determined for the $\phi = 0^\circ$, and transformations described by formulas (5)÷(8) are performed when comparing the signature with data from other directions.

To facilitate understanding of the form of the multi-dipole model, the authors prepared Fig. 21. Dipoles are represented by ellipsoids with positions (x_i, y_i, z_i). The size of each ellipsoid depends on the magnetic moment $(m_{x,i}, m_{y,i}, m_{z,i})$ associated with the dipole. These quantities are linearly scaled with respect to the largest moment. The interpretation is that individual dipole is the source of the local magnetic field, and their superposition constitutes the magnetic signature of the ship.

4. Simulation analysis

Determining the values of the signatures depends on too many factors to consider separately, hence it was decided that a Monte Carlo type simulation will be an appropriate approach to the analysis of the effect of an error in determining the ship position relative to the measuring device on the form of the magnetic signature. The idea behind this approach, shown in Fig. 22, consists of three sections (marked with different colors): (1) gathering measurements, (2) developing statistical distributions based on the measurements, and (3) using the developed distributions to generate thousands of simulation scenarios.

For the purpose of the simulation study, three measurement

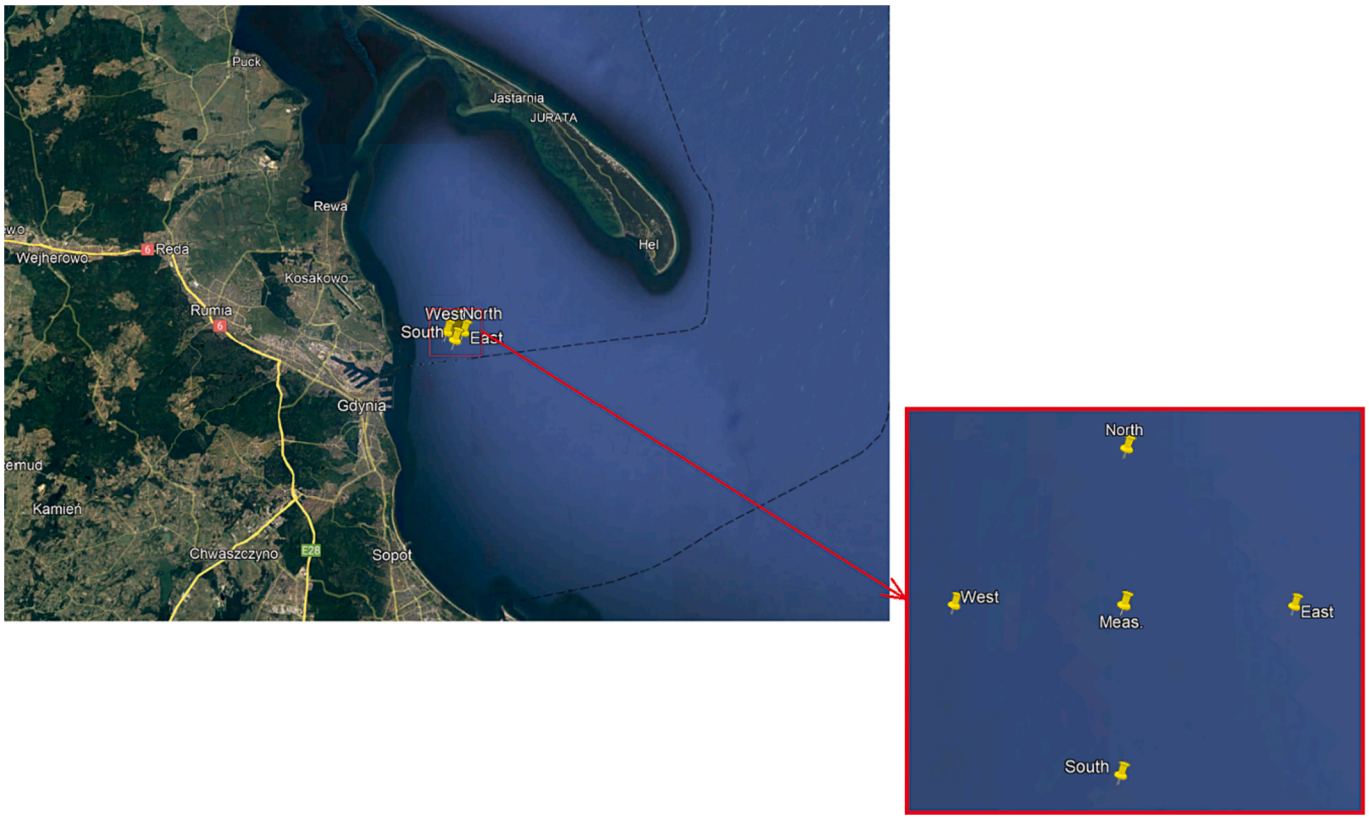

Fig. 12. Outline map with boundary points.

Fig. 13. Hybrid boat with bow measurement system.

campaigns described earlier were used: (1) magnetic measurements while the ship is moving with position determination using the Furuno receiver, (2) position measurements using two Furuno and Leica GPS receivers at sea while the RIB is moving, and (3) comparing the readings of two GPS receivers remaining at the same location over a 24-hour period.

In the analysis, the magnetic field measurements made are treated as the reference and are not subject to any corrections. The change in ship position relative to the original trajectory and the measuring device and its effect on the form of the magnetic signature obtained using the multi-dipole model is considered. In order to propose corrections to the original trajectories, the analyses of statistical distributions of differences between GPS receivers were carried out. By appropriate sampling the distributions of the differences of GPS receiver readings, a model of the

Fig. 14. View of hybrid boat trajectories consistent with ZODIAK transits during the 2019 survey.

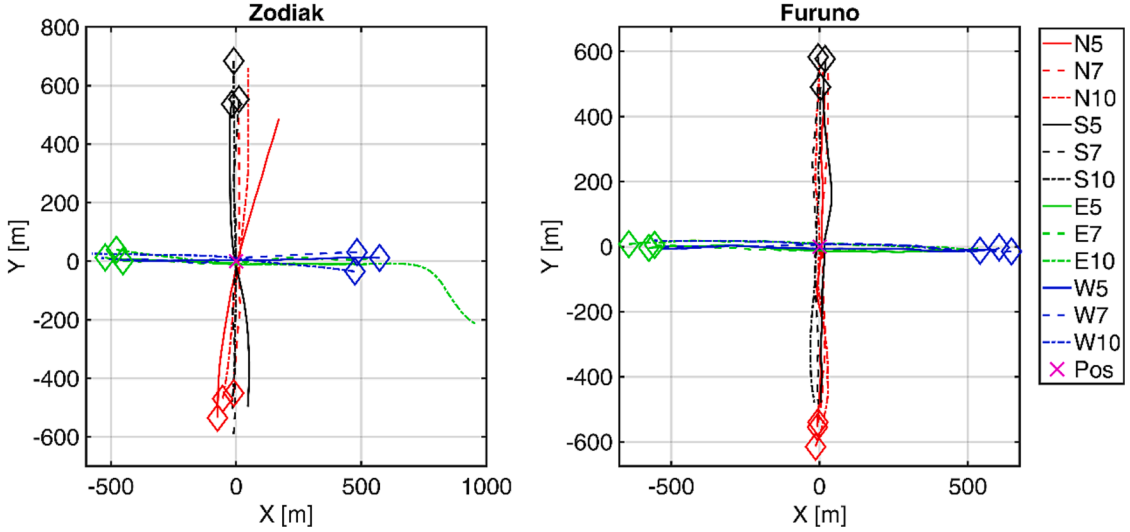

Fig. 15. Trajectories of transits of ZODIAK measurements (left) and additional GPS receiver accuracy measurements (right). Coordinates (0,0) correspond to the position of the underwater measurement module

error in determining the stationary position of the measuring device and the error in ship movement was obtained. These random error realizations were then superimposed on the original trajectories of *Zodiak* and, together with the original magnetic flux density values, applied as the input to a multi-dipole model to be used to simulate virtual potential magnetic signature forms. For a sufficiently large number of simulations, their successive repetitions with a new position error realization should explore all the search space of the actual ship passage and build a family of possible signatures, thus providing the information on the impact of inaccuracies in position determination on the quality of the obtained signatures.

Detailed description of the Fig. 22:

A. Measurements
   a. Zodiak experiment performed in 09.2019 in Gulf of Gdańsk:
      i. magnetic measurements,
      ii. moving ship geographical position measurements,
      iii. magnetometer position measurements,
   b. GPS stationary experiment performed in 01.2021 in position 54,54 N 18,54E – Stationary measurements with two GPS receivers:
      i. Zodiak Furuno receiver,
      ii. geodetic reference reciver,
   c. GPS in motion experiment in 06.2021 – Sea measurements in Gulf of Gdańsk with two GPS receivers:
      i. Zodiak Furuno receiver,
      ii. geodetic reference reciver,
B. Development of statistical distribution
   a. For stationary
      i. statistical analysis of position error,

Table 1
Transition parameters for ZODIAK and hybrid boat.

Run name	Run No.	Heading [°]	*ZODIAK*			Hybrid boat		
			Speed at CPA [kn]		CPA [m]	Speed at CPA [kn]		CPA [m]
			Target	Real		Target	Real	
N5	1	0	5	4,6	1,4	5	4,8	3,8
E5	2	90	5	5,3	12	5	5,2	9,7
S5	3	180	5	5,1	9,4	5	5,3	11,8
W5	4	270	5	4,9	1,4	5	5,5	3,8
N7	5	0	7	7,8	7,3	7	7,1	4
E7	6	90	7	7,8	6,7	7	7,1	12
S7	7	180	7	7,2	4,6	7	6,9	15,8
W7	8	270	7	7,7	9,4	7	7	6,5
N10	9	0	10	9,9	7	10	10,2	5,7
E10	10	90	10	9,8	10	10	10,5	9,9
S10	11	180	10	9,7	6	10	9,8	5,8
W10	12	270	10	10	8,4	10	10,1	7,6

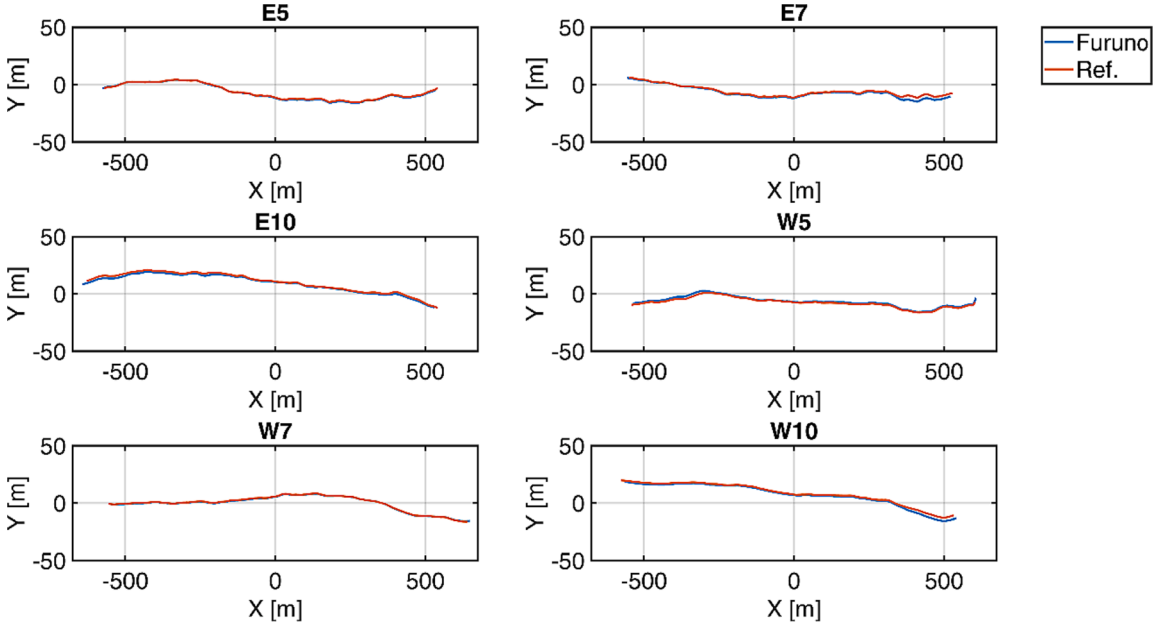

Fig. 16. GPS tracks recorded with two receivers (red - reference, blue - tested) on courses E and W. (For interpretation of the references to colour in this figure legend, the reader is referred to the web version of this article.)

ii. development of error probability distributions for determining stationary position of magnetometer,

b. For ship in motion
   i. statistical analysis of position error,
   ii. development of error probability distributions for determining moving ship position

C. Monte Carlo Simulation (1000 times)
   a. Error generator based on distributions – generator based on previously obtained probability distributions regarding the position of the moving ship relative to the stationary measuring device,
   b. Overlaying errors on original data - Overlaying the original trajectories of the ship and the position of the measuring device with errors modelled on the basis of the experiment with the comparison of GPS indications,
   c. Magnetic signature determining – determination of magnetic signatures based on original magnetic measurements and modified by the error of ship's position relative to the measuring device modelled using a multi-dipole model,
   d. Collective magnetic signatures presentation – superposition of single form of magnetic signatures from a particular ship passages to obtain the entire spectrum of possible ship passages and signature form.

4.1. Analysis of the obtained differences between reference receiver and GPS receiver used on stationary ZODIAK (positioning error model for the measuring device)

The spread of GPS receiver readings is shown in Fig. 9. That graph only shows the area in which the results were located but says nothing about the frequency of a given result. It can be seen that the largest errors reach a few meters for each coordinate. For the purpose of modeling the error contributed from the measuring device position, statistical distributions of the errors by x, y coordinates were created. It can be seen in the distributions shown in Fig. 23 that the most common situation was when both receivers indicated the same position, while errors with large values were rare. Sampling these distributions is the approach used in the article to account for an error in determining the position of the measuring device in the simulations.

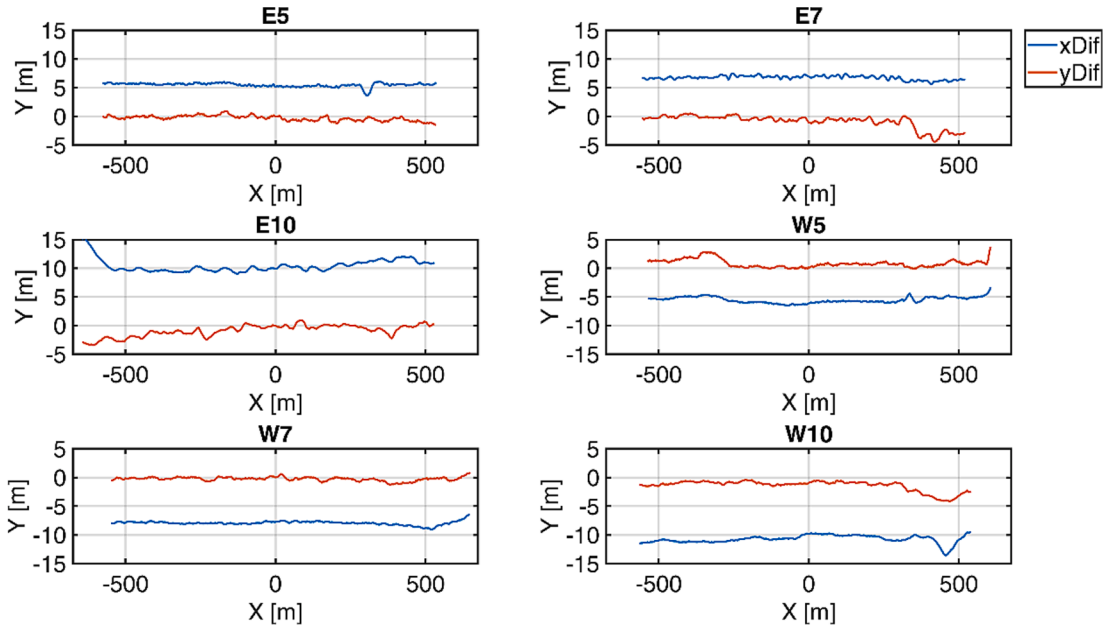

Fig. 17. Differences between the GPS tracks of the reference receiver and the tested receiver on courses E and W.

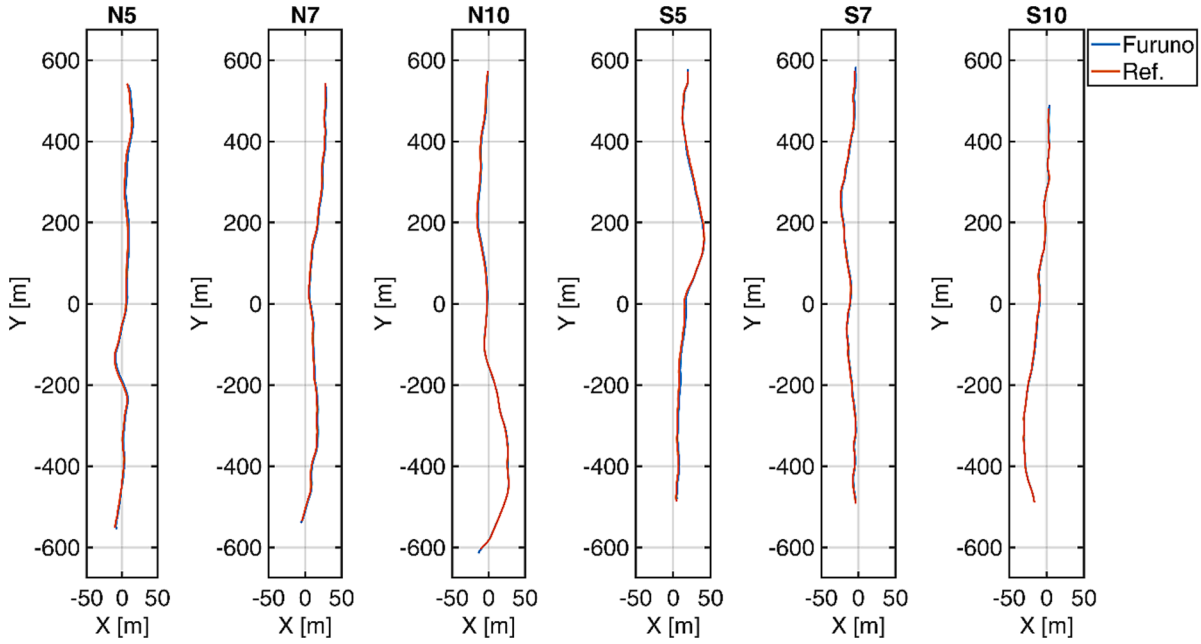

Fig. 18. GPS tracks recorded with two receivers (red - reference, blue - tested) on courses N and S. (For interpretation of the references to colour in this figure legend, the reader is referred to the web version of this article.)

4.2. Analysing differences between reference receiver and GPS receiver used on ZODIAK during its movement

The results of GPS measurements were analyzed in various ways. Fig. 24 shows the recorded differences between the readings of GPS receiver by courses N<->S and W<->E, and by coordinates x and y.

Analyzing the graphs in Fig. 24, it can be observed that in addition to the noise that appears at each passage, a constant "offset" has place at coordinates that follow the ship's course, i.e., an offset in the y-coordinate at the north–south and south-north directions, and an offset in the X-coordinate at the east–west and west-east transitions. What is more, this offset is proportional to the ship's speed. We can also observe that the indications of the Furuno receiver are ahead of the actual position.

The calculated offsets for the 12 ship passes are summarised in the Table 2. Samples were recorded at a frequency of 1 Hz over a distance of at least 1 km. Consequently, a different number of samples were recorded for the different speeds (10, 7 and 5 knots), as can be seen in Fig. 22. For the speed of 10 knots, the mean values of the position differences were determined from about 200 samples, for 7 knots from about 300, and for 5 knots from about 400 samples. At each pass, the number of samples varied slightly within a given speed.

After removing (subtracting) the mean of the samples recorded for the y-coordinate in the N-S/S-N relationship and for the x-coordinate in the E-W/W-E relationship, histograms were plotted to get an idea of the nature of error distributions. The results are shown in Fig. 25.

For the purposes of error modeling, it will also be useful to know by

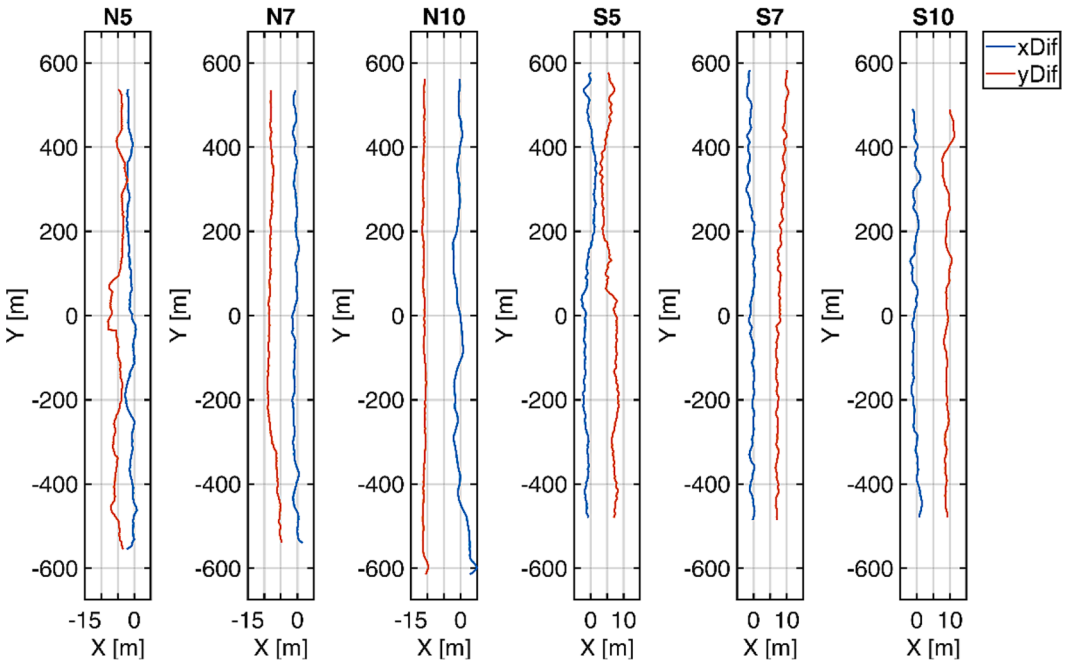

Fig. 19. Differences between the GPS tracks of the reference receiver and the tested receiver on courses N and S.

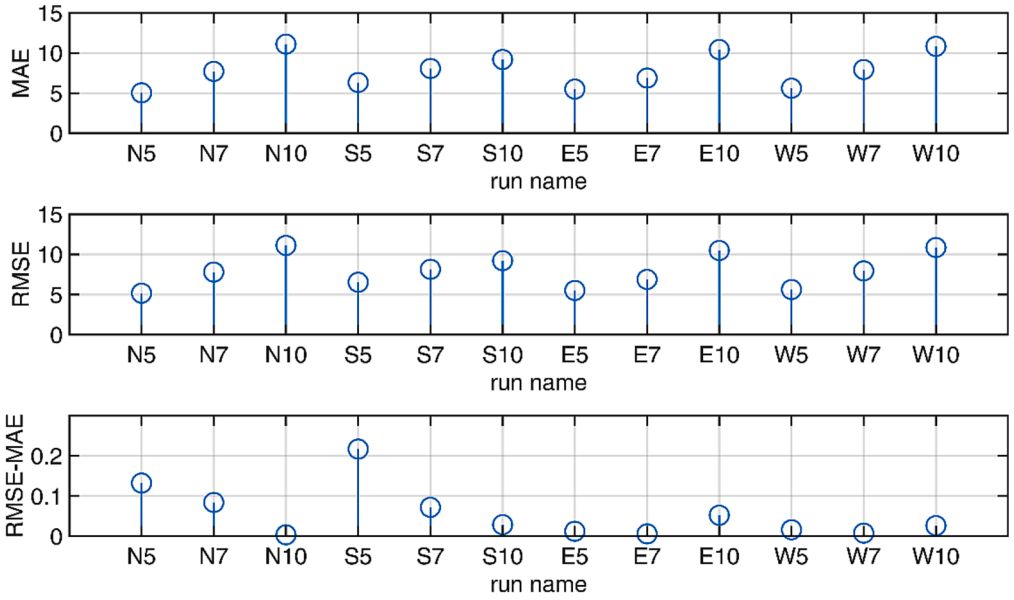

Fig. 20. Summary of mean and root mean square error values for each vessel passage.

how much the value of the difference between the samples can change. This information can be obtained from Fig. 26 and Fig. 27.

4.3. Approach to modeling ship transitions

Offset model. The presented approach to modeling ship transitions is black-box in nature, that is, it abstracts from the actual nature of the GPS error phenomenon. It is based solely on the data collected as a result of the experiments described earlier. Obviously, the results are local in nature, i.e., they refer to the place and time at which the experiment was conducted.

N-S/S-N and W-E/E-W transitions were modeled separately but following the same principle. Due to the offset occurring, the error for x and y coordinates was also modeled separately.

The phenomenon of displacement (offset) along the direction in which the ship is moving was the least represented, because there are only 12 subsets in the entire measurement data set from which its value can be inferred. However, strong patterns are observed. The method used to model the offset consisted in determining the average value of this offset for each speed based on 4 values for each direction. The maximum amplitude (the difference between the average and the maximum value) for each velocity was then determined. As a rule, the model uses the determined average to which a random value from zero to +/- amplitude is added. For example, for the speed of 7 kn, the average was determined from the set (N7, W7, S7, E7), and the maximum amplitude from among the same waveforms. The model sums the value of the determined average and a random variable from the range (-1 ÷ 1) multiplied by the value of the determined amplitude. The

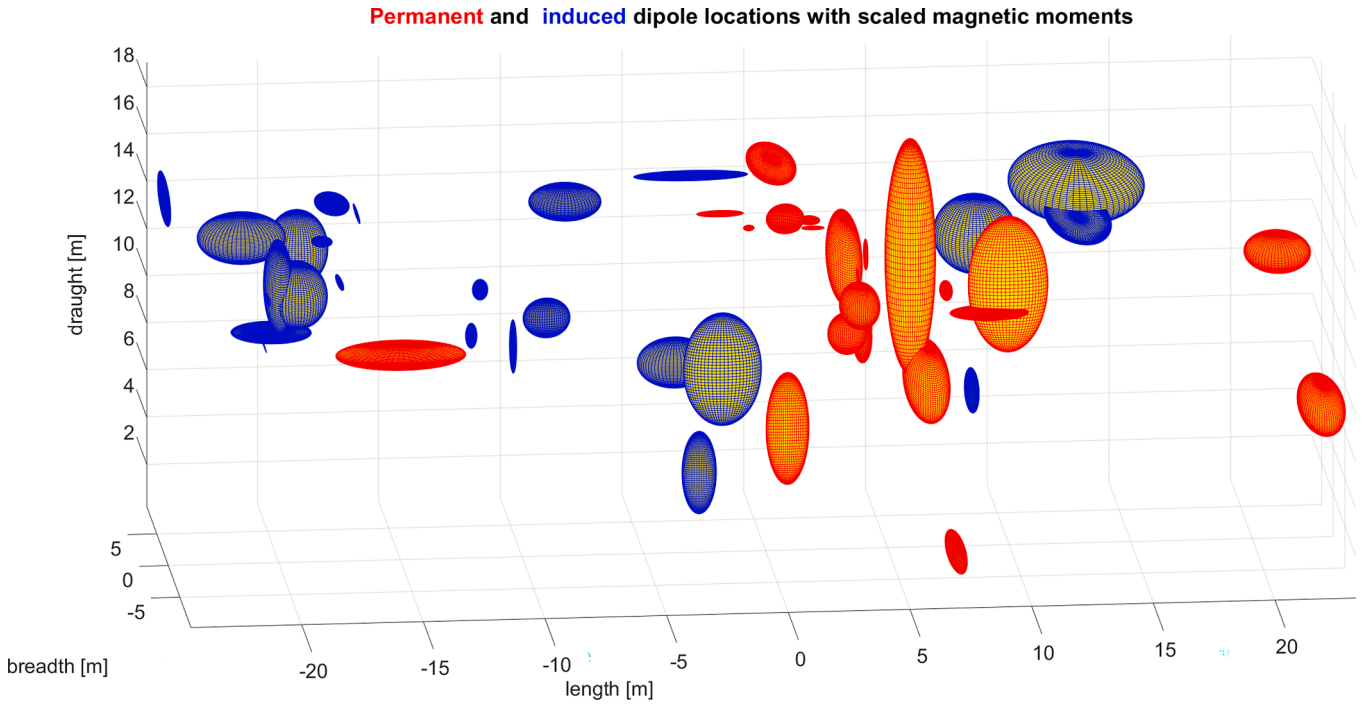

Fig. 21. Graphical representation of the multi dipole model for the Zodiak ship.

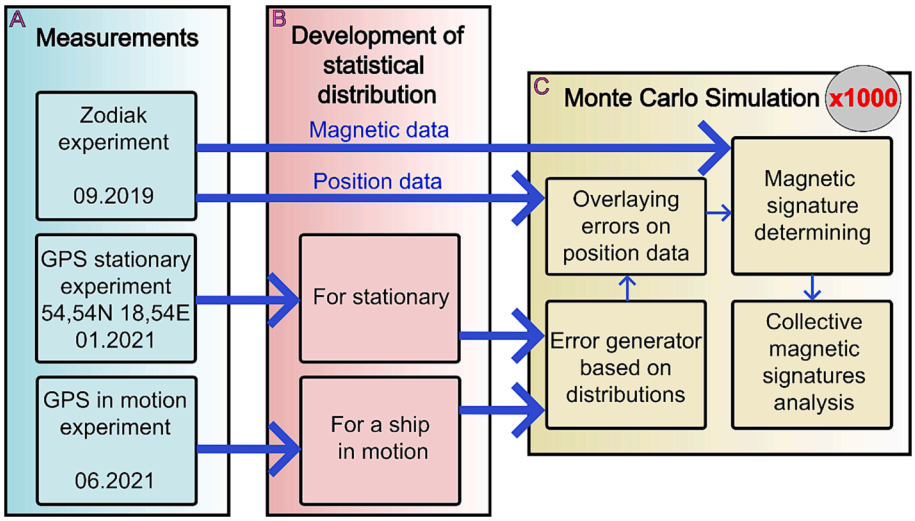

Fig. 22. Workflow of simulation analysis.

value determined in this way is subtracted from the position indication in the original data obtained from the Furuno receiver to remove the observed error and make the ship's position realistic.

Noise model. The noise model is based on the graphs shown in Fig. 24, Fig. 25. They show that each error has a specific, different statistical distribution. From the graphs in Fig. 26, Fig. 27 we can determine the limits of change within a single sample. Moreover, analyzing the distributions of differences between the readings of two GPS receivers, we can conclude that the modeling approach should take into account the following aspects:

- the next step is to be related to the previous one, because the vessel cannot change its position drastically,
- the permissible step between samples should be given parametrically to be able to give the actual position change resulting from the analyses,
- different realizations of the simulation scenarios should be random,
- this randomness, however, should be determined by a preset distribution.

Various approaches to modeling the process of concern have been proposed, e.g. [25,26]. Comprehensive descriptions of the stochastic modeling approach can be found in [27] and [28]. In particular, the reader will find discussions of Monte Carlo modeling issues in [29] and [30,31], among other sources.

Here, the stochastic Metropolis Monte Carlo Markov Chain (MCMC) method, originally described in [32] and later developed in [33], was chosen. This method is based on Markov chains, therefore it guarantees that the next value is related to the previous one, and the step length and, consequently, the value of the change is controlled by the adopted method parameter. The properties of the MCMC method make it possible to model noise with a specific probability distribution known in

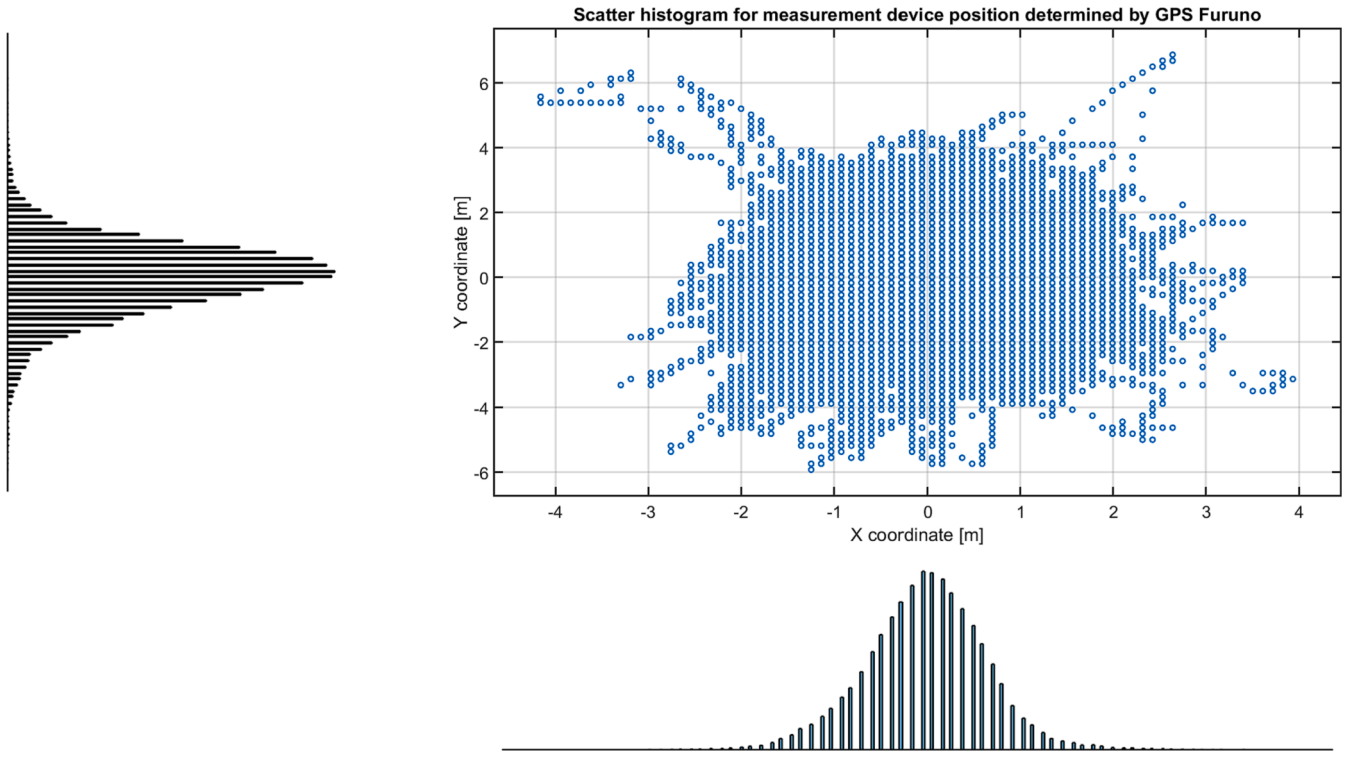

Fig. 23. Scatter histogram for Furuno GPS receiver stationary position measurement.

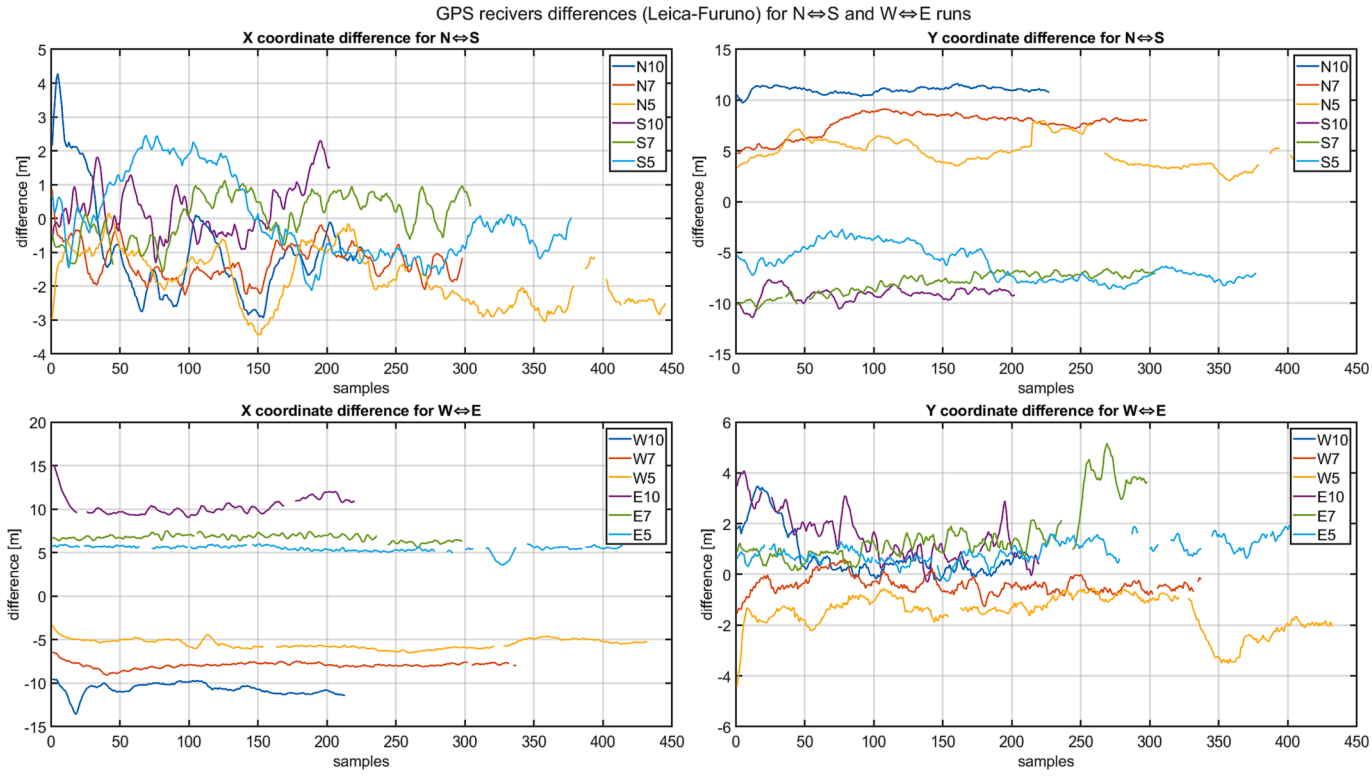

Fig. 24. Difference between position measurements recorded by Furuno and Leica GPS receivers, broken down into N<->S, W<->E runs and x, y coordinates.

Table 2
Offsets calculated as mean values.

	N (y-coord offset)	S (y-coord offset)	W (x-coord offset)	E (x-coord offset)
Speed 10 kn	11.00 *m*	−9.15 *m*	−10.69 *m*	10.35 *m*
Speed 7 kn	7.67 *m*	−7.99 *m*	−7.93 *m*	6.73 *m*
Speed 5 kn	4.78 *m*	−6.1 *m*	−5.48 *m*	5.47 *m*

advance. The Monte Carlo approach indicates that it is not only one realization of noise which will occur, but many, which together compose the simulation experiment.

The Metropolis – Hastings [34] algorithm can be described with the following rules:

for $i = 0..N$ do

1. *Sample* x^c *from* $P(x^c|x_i)$
2. *With accptanceprobability* $\alpha(x^c, x_i) = min\,(1, \frac{T(x^c)P(x_i|x^c)}{T(x_k)P(x^c|x_i)})$ *assign* $x_{i+1} = x^c$
3. *In other case assign* $x_{i+1} = x_i$

(9)

where:$P(x)$– proposal distribution$T(x)$– target distributionx_0– initial guessx_i– sample for i algorithm iterationx^c– candidate

This algorithm generates a sequence of iterates $\{x_1, x_2, \cdots, x_N\}$ with approximate distribution T for sufficiently large N.

A well-known property of the MCMC algorithm is that in order to sample according to the T distribution, a burn-in phase is needed the limit of which cannot be determined theoretically. Generally, the implementation problems are encapsulated in the following issues: selecting the step of the method (represented by the variance of the distribution P), determining how long the burn-in phase lasts, and verifying that we get a good reproduction of the distribution T. The length of the step cannot be too short, nor can it be too long. Here, its value was derived as equal to 0.2 m from the analysis of the ship position change (Fig. 26, Fig. 27). Moreover, as a result of simulation experiments, it was found that high agreement is obtained after discarding 10 %-15 % of initial samples in the set. Therefore, a certain margin was assumed, and 20 % of samples were oversampled and the first ones were removed from the set. Fig. 28 compares the original noise distribution for each direction and its unit realization obtained using the MCMC sampling. It can be seen that these distributions are in good agreement. Certainly, as is typical in Monte Carlo methods for each of hundreds of noise realizations, the distribution will be slightly different but always based on the T distribution observed in the measurement results. In turn, Fig. 29 compares the ship transitions according to the modeled errors (one realization out of 1000) with the original transitions.

4.4. Determining the parameters of the multi-dipole model

According to the scheme shown in Fig. 22, for each realization of the modified passage, the values of magnetic signatures were determined using a multi-dipole model. These issues were described in detail in [5] and [6] and are not the main topic of this article, but are briefly cited here to familiarize the reader with the methodology. Using the optimization procedure presented in [5], the multi-dipole parameter values are determined to minimize the distance between the model outputs and the measured signatures. The optimization problem is defined with (10)

$$\min_{\Omega\in\{\Omega_1,\cdots,\Omega_{n+m}\}} J_G = \sum_l \sum_d \sum_{j=1}^{501} \left(B_{l,d}^{ref}(j) - B_{l,d}^{model}(j, \Omega, \phi(d)) \right)^2 \tag{10}$$

subject to:

$$\underset{i \in (1, m+n)}{\forall} \Omega_i^{\min} \le \Omega_i \le \Omega_i^{\max} \tag{11}$$

where:

$$\underset{i \in (1, m+n)}{\forall} \Omega_i \in \{m_{x,i}, m_{y,i}, m_{z,i}, x_i, y_i, z_i\} \tag{12}$$

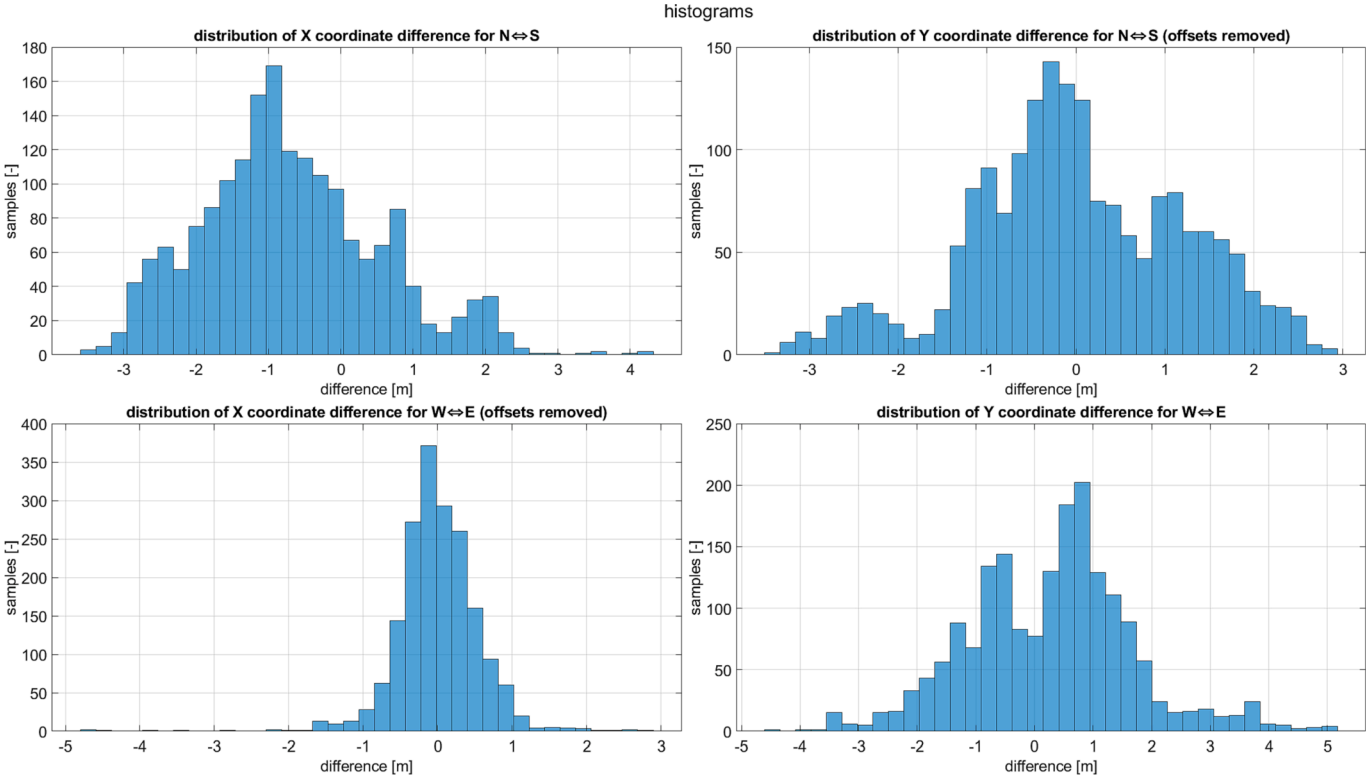

Fig. 25. Distributions of differences between GPS receivers after removing the mean values from each pass.

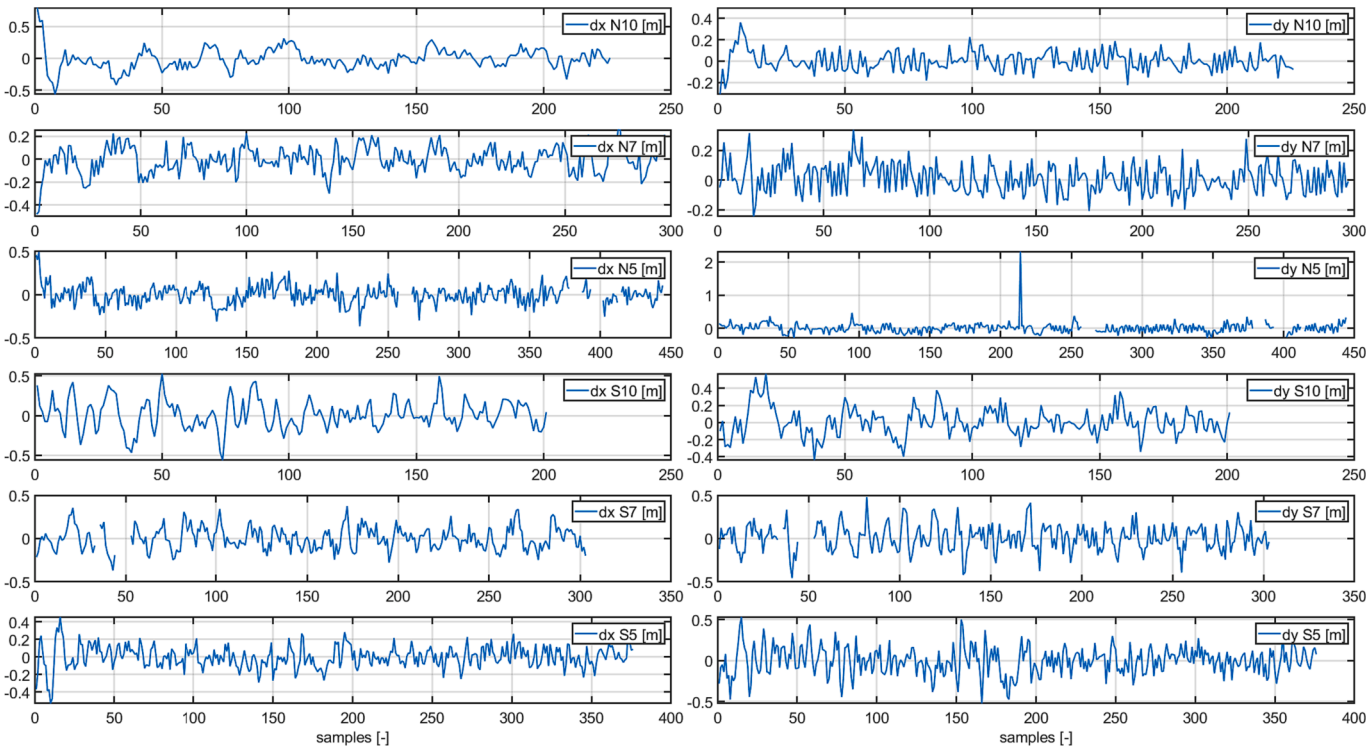

Fig. 26. One-step position difference for N-S and S-N runs.

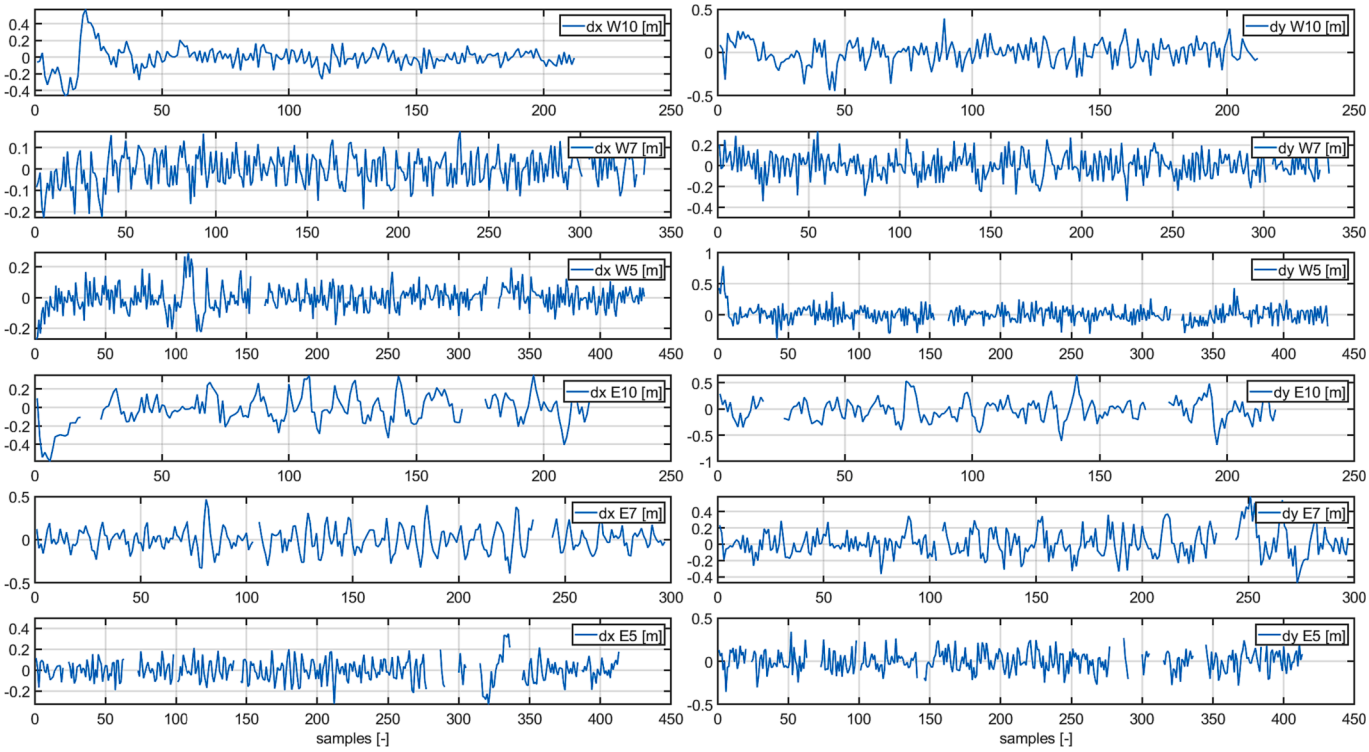

Fig. 27. One-step position difference for W-E and E-W runs.

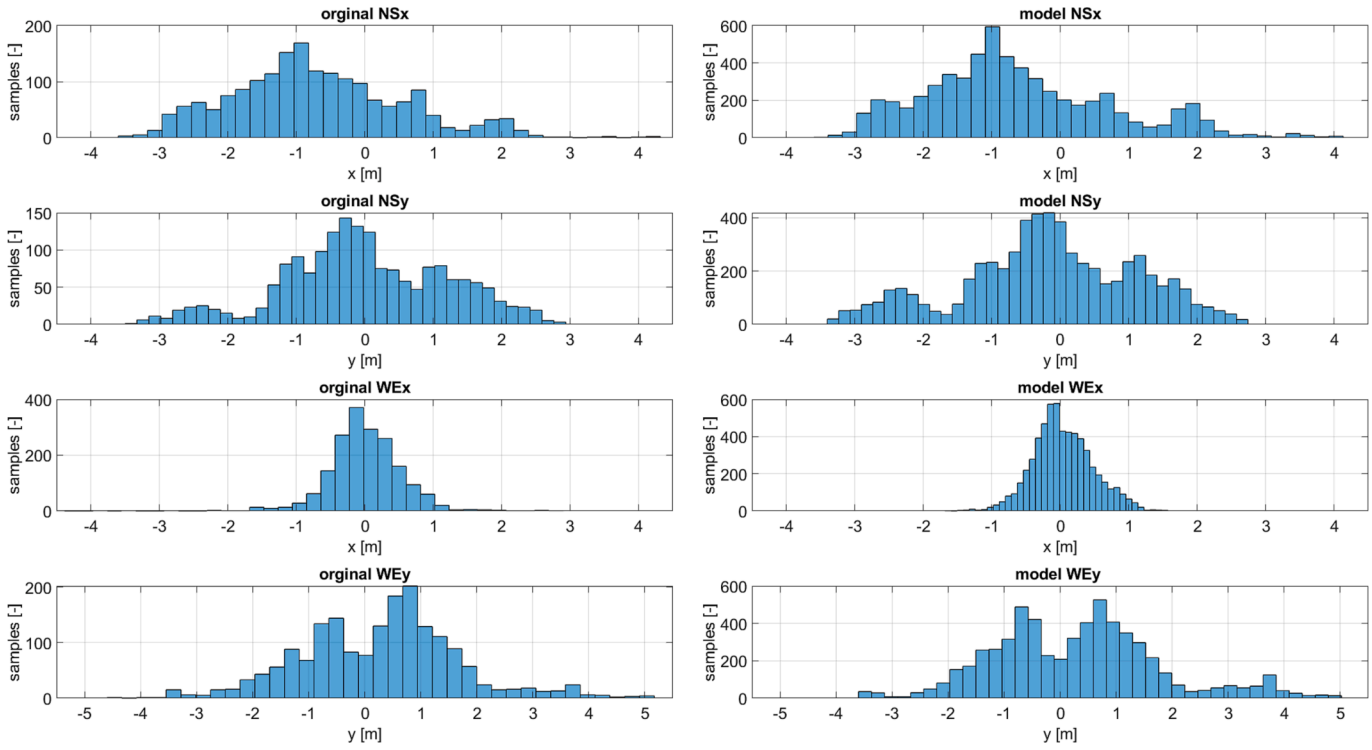

Fig. 28. Comparison of original error noise distribution (left) with that generated by the MCMC method (right).

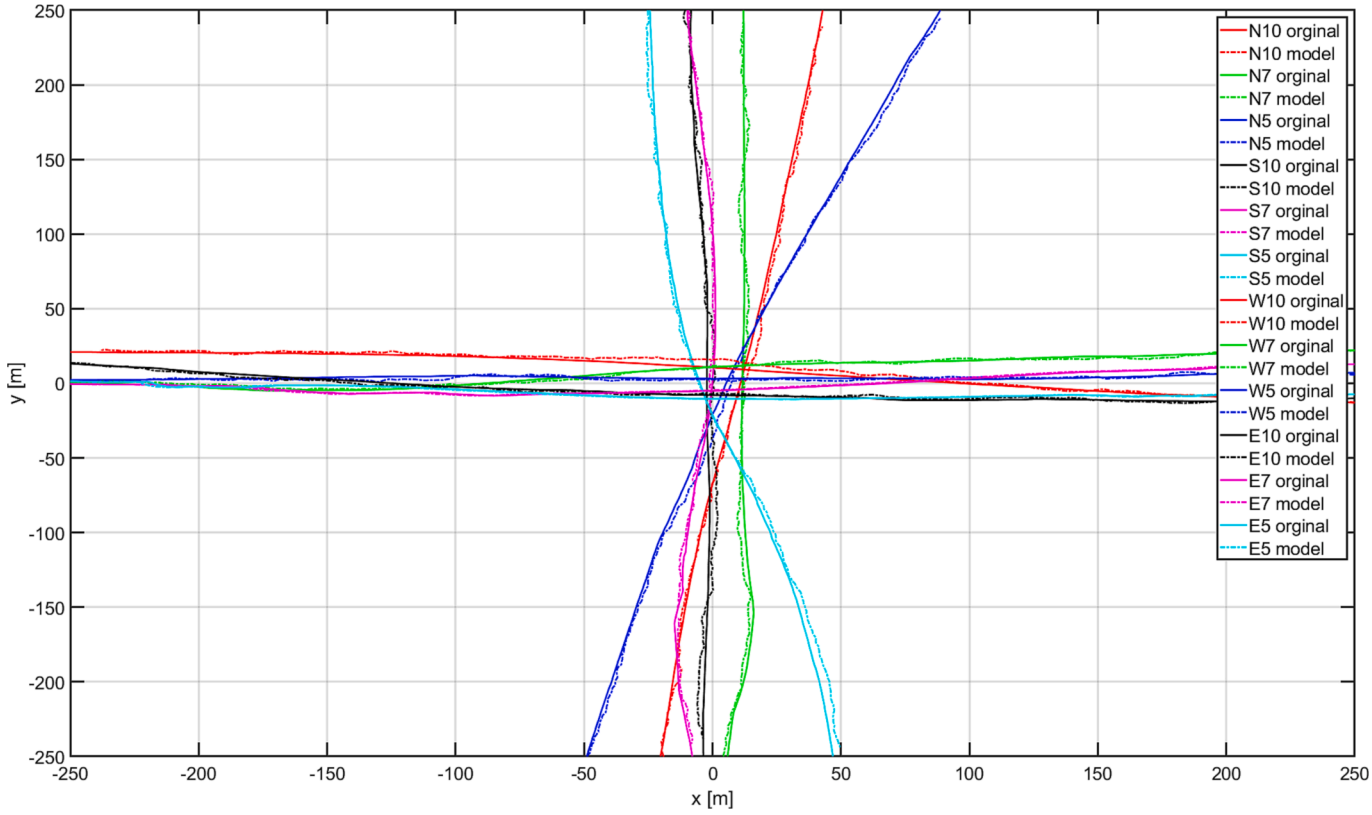

Fig. 29. Ship's original passages (marked with solid lines) and ship's passages modified according to error distributions (dotted lines).

$$l \in \{x, y, z\} \tag{13}$$

$$d \in \{N10, E10, S10, W10, N7, E7, S7, W7, N5, E5, S5, W5\} \tag{14}$$

where J_G is the objective function, n is the number of permanent dipoles, m is the number of induced dipoles, l stands for a set of x, y, and z components of magnetic field, d means an analysed dataset - in presented ship Zodiak case, all available data for 4 directions and for 3 ship speeds, j is the number of analysed samples, $\varphi(d)$ describes the ship heading, Ω is the vector of all decision variables defined for all considered dipoles, $\Omega_i^{\min}$, $\Omega_i^{\max}$ are the vectors of minimal and maximal bounds for the decision variables subset Ω_i defining *i-th* dipole.

Determining model parameters using optimisation is often named model training (FIT). Model validation referred to as cross-validation (CV) is performed on data that was not used for training. In this article as successor of [5] the leave-one-out (LOOCV) approach is also applied. It consists in using all data from the available set, but data from one path is used for verification purposes. There are dozen such scenarios with the data from 11 sets used for training and 1 for validation. This approach increases the amount of computation, but allows for a fair assessment of model quality.

A nonlinear least-squares (nonlinear data-fitting) solver using TRR (Trust-Region-Reflective) optimization [21] algorithm was applied to solve (10). Calculations were performed in the Matlab package using the *lsqnonlin* function. In order to study the influence of initial conditions, experiments with random initial conditions were performed in [6] to investigate their impact on stability, repeatability of results and the problem of possible getting stuck in local minima. Regardless of the initial conditions, similar results of the optimization process were obtained. It was found that the task was well conditioned. Another important aspect of conducting the optimization process is determining the number of iterations of the algorithm or, more generally, the conditions for stopping the procedure. The number of iterations of the optimization algorithm may influence the phenomena of overfitting or overtraining. The principle of determining the number of iterations of the optimization procedure by analyzing FIT learning curves and CV verification is presented in [5]. In the parameter setting procedures [5], L1 and L2 regularization procedures were also considered, the operation of which caused various effects on the dipole parameters, but did not significantly affect the achieved signature reproductions.

The result of calculations for one scenario of a set of ship passages is 12 sets of dipoles describing the distribution of the magnetic field. As a result of the experiments, it was assumed that the appropriate number would be 30 permanent and 30 induced dipoles. Each dipole is described by 6 parameters *x, y, z, mx, my, mz*. The results are saved in files for later use. In total, the Monte Carlo analysis undertaken in this article using 1000 different ship routes resulted in 12,000 files with dipole parameters. The calculation time on a computer with an i9-13900 K CPU and 128 GB RAM was 12 days, 5 h and 6 min.

4.5. Assessment of results and error comments

The superimposition of all signatures obtained using the stochastically simulated ship position error on the original transitions is shown in Fig. 30, Fig. 31, and Fig. 32. Analyzing the presented waveforms, it can be observed that the fit of the B_z component is very good, along with narrow ranges of the signature waveforms regardless of the variation of the ship's routes, which is understandable as this component has the largest values and dominates the optimization criterion.

Very good matches and narrow signature ranges can also be observed for the B_x component of the N and S paths, and for the B_y component of the E and W paths. Here, we can see the fundamental effect of ship position on the E, W paths in the case of the B_x component, and on the N and S paths for the B_y component. A change of several meters in ship position causes the signature to bend and change sign (cases E5 and E10). This clarifies the doubts in the article [5] about the origin of errors in the model versus the measurement. To analyse the sensitivity of the magnetic signature to the error in determining the exact passage of the ship, a model of *Zodiak* has been developed in FEM software. The perturbations of the x and y positions were made by substituting the shifted coordinates into equation (3). Fig. 33 and Fig. 34 show the effect of the error in determining the value of the coordinate orthogonal to the ship's motion on the B_x and B_y components of the magnetic signature in the north direction, while Fig. 35 and Fig. 36 show the same effect on the B_x

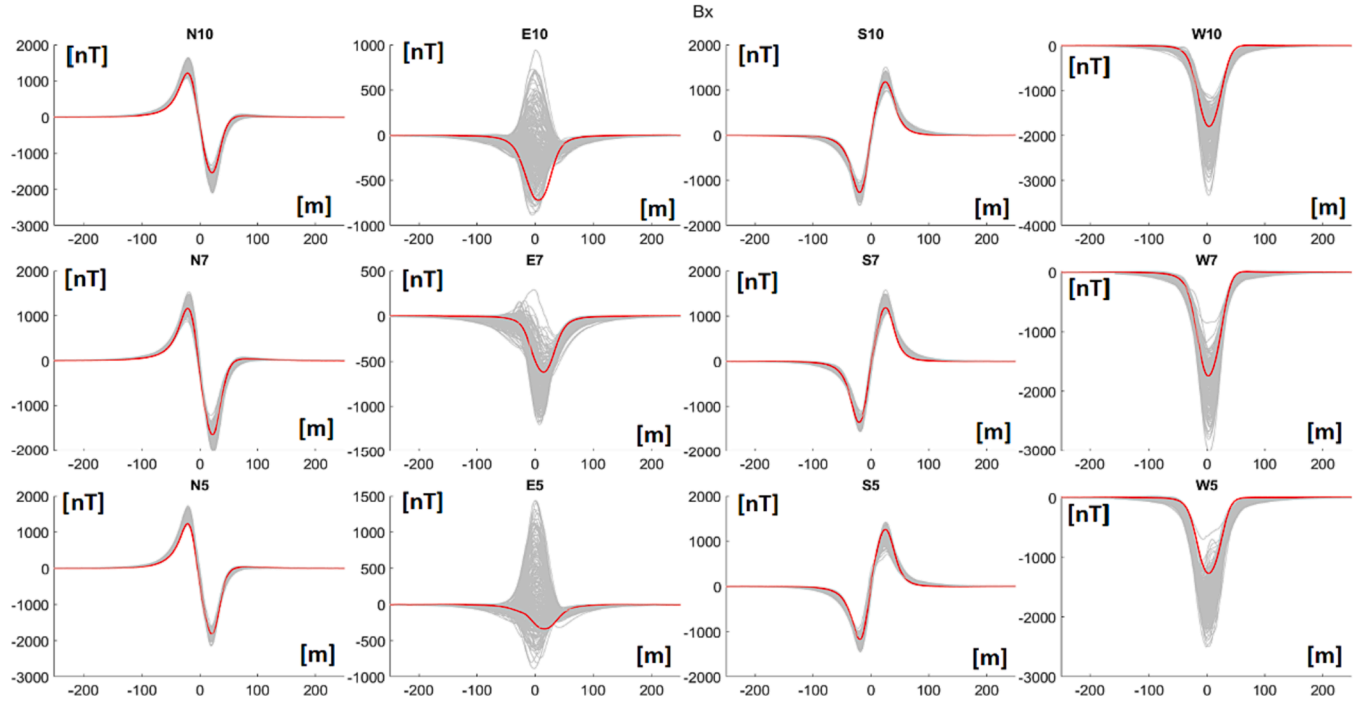

Fig. 30. Basic method results - Bx component of MF (red – measured, blue - Monte Carlo simulation). (For interpretation of the references to colour in this figure legend, the reader is referred to the web version of this article.)

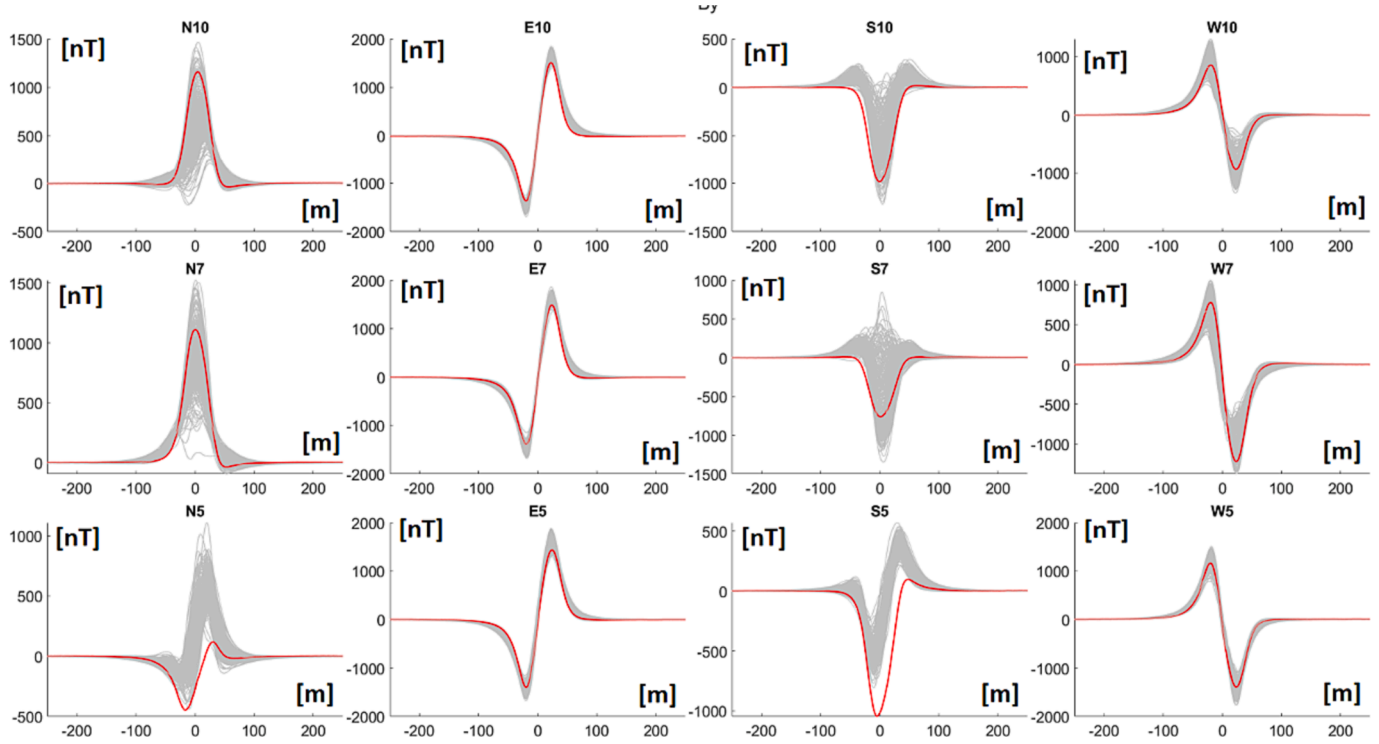

Fig. 31. Basic method results - By component of MF (red – measured, blue - Monte Carlo simulation). (For interpretation of the references to colour in this figure legend, the reader is referred to the web version of this article.)

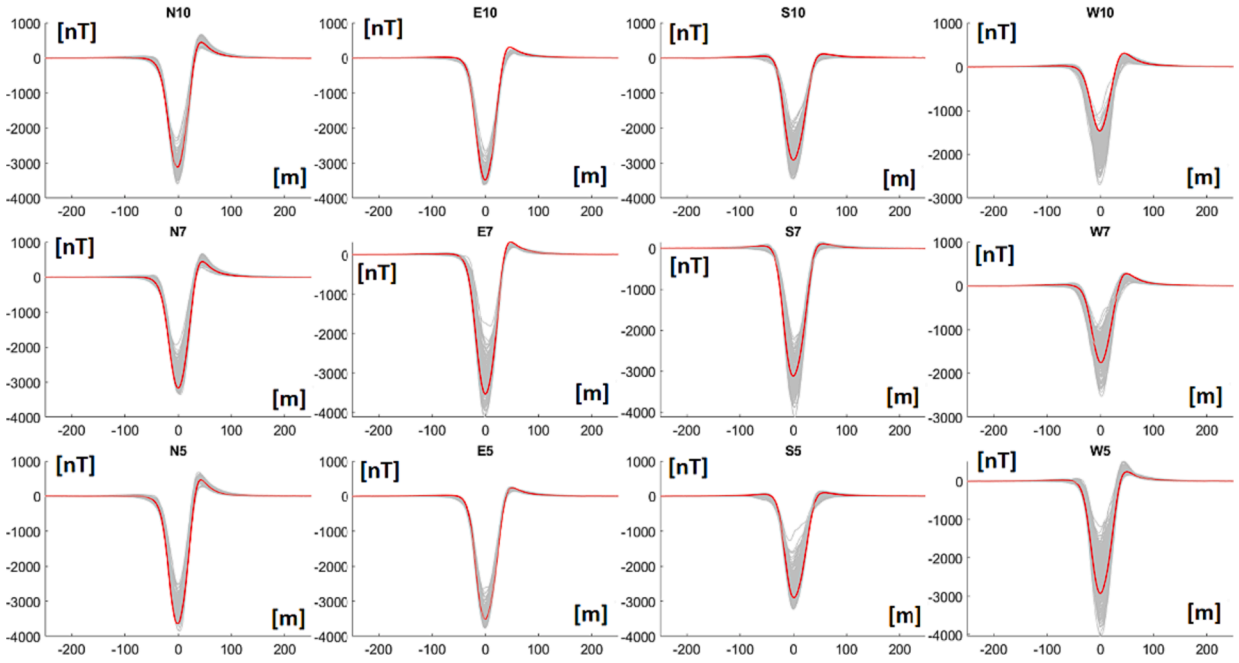

Fig. 32. Basic method results - Bz component of MF (red – measured, blue - Monte Carlo simulation). (For interpretation of the references to colour in this figure legend, the reader is referred to the web version of this article.)

and B_y components in the east direction. Fig. 33 reveals that for the north direction and the B_x component, a change in the x-coordinate does not bring a change in the nature of the signature, but only changes its value. In contrast, Fig. 34 clearly shows that a change in the value of the x-coordinate has a major effect on the nature of the signature. A similar relationship can be seen in Fig. 35 and Fig. 36. It should be noted, however, that the ship's transitions recorded during the measurements usually avoided the point (x = 0, y = 0) (see Fig. 29), as a result of which the signatures based on real transitions will not always have such clear differences as those in Fig. 33, Fig. 34, Fig. 35 and Fig. 36, as the simulated transitions may be situated on the same side relative to the measuring device for a significant part. In view of the above considerations, the results obtained from MCMC simulation are justified in comparison with the results of the model analysis. The presented basic

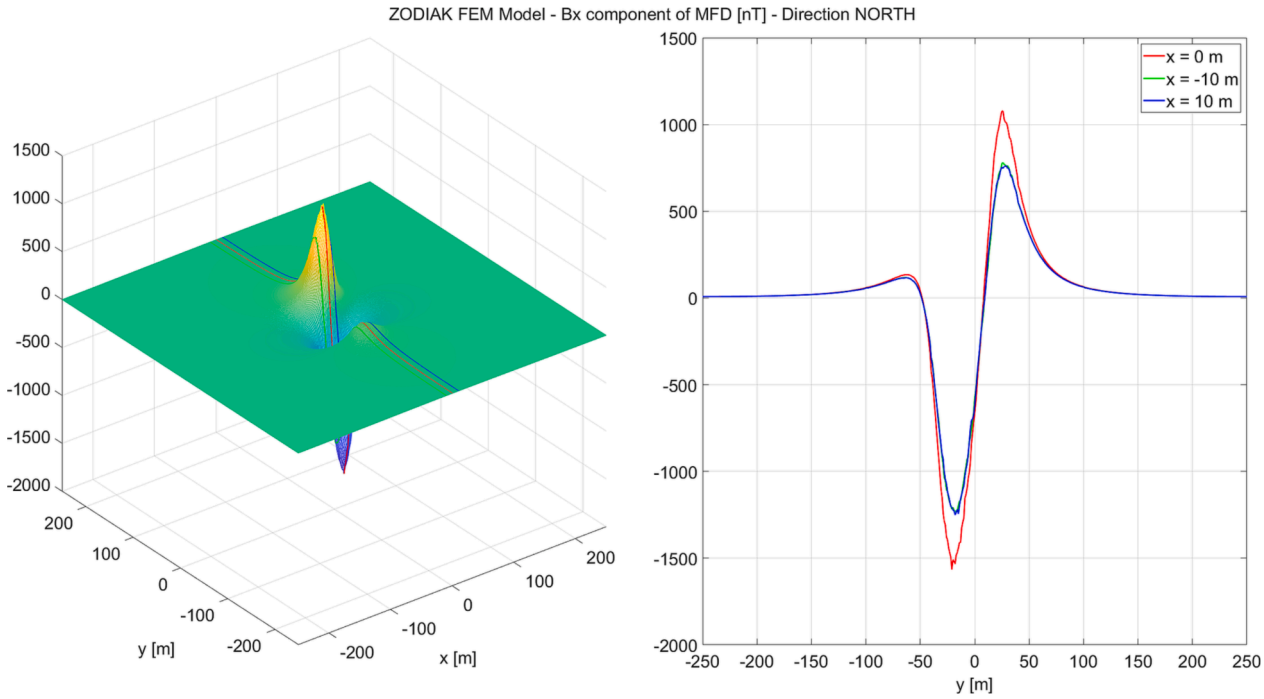

Fig. 33. The effect of the coordinate orthogonal to ship's motion on Bx component for north direction.

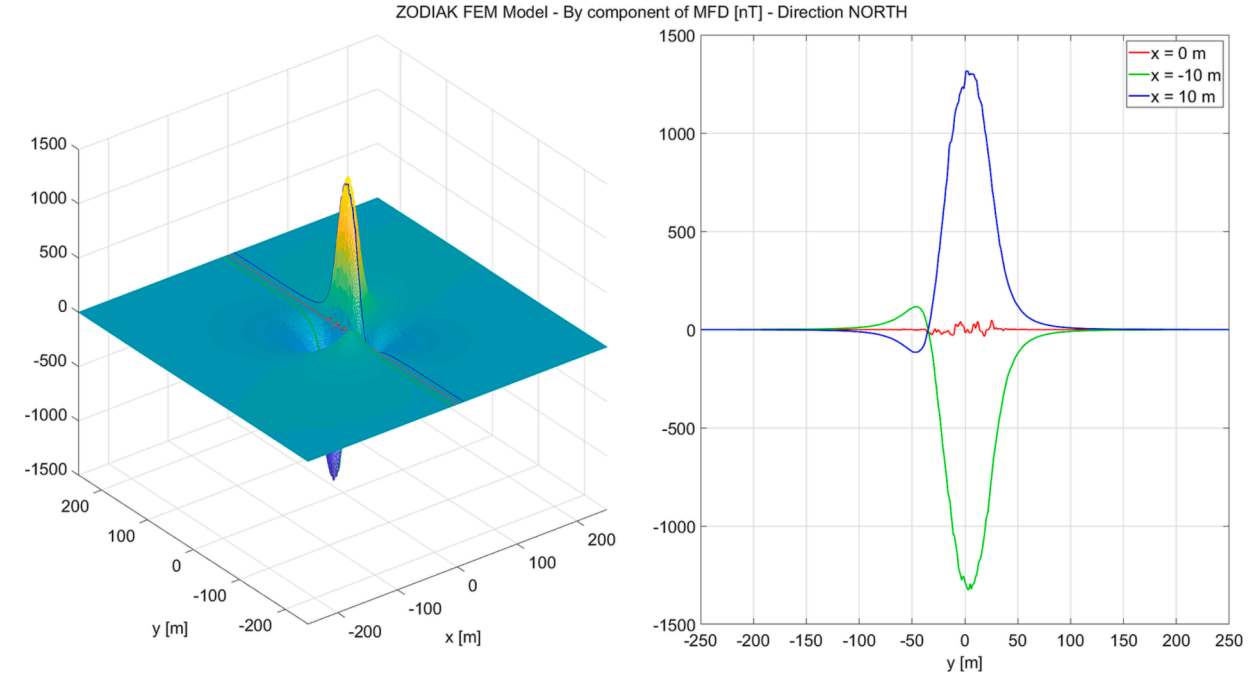

Fig. 34. The effect of the coordinate orthogonal to ship's motion on By component for north direction.

approach, when used, indicated a significant effect of the position determination error on the quality of signatures, but did not allow to simulate all conditions under which a waveform consistent with the measurements was obtained from the model. That is why the study was complemented with extended approach.

4.6. Extended method

Setting the measuring module on the bottom of a given body of water in a specific geographic position is subject to a certain inaccuracy resulting from environmental conditions, such as hydrometeorological and bathymetric conditions that directly affect the setting process, which can become very difficult in the case of elevated sea state, increased swell, and wind speed.

The procedure for setting up an object on the bottom requires the use of a vessel that also performs the transportation function. The type of the vessel used for this purpose determines the method to stabilize its position relative to the indicated geographical position where the underwater object is to be placed. A vessel equipped with a thruster system that assists maneuvering in difficult conditions can dynamically correct

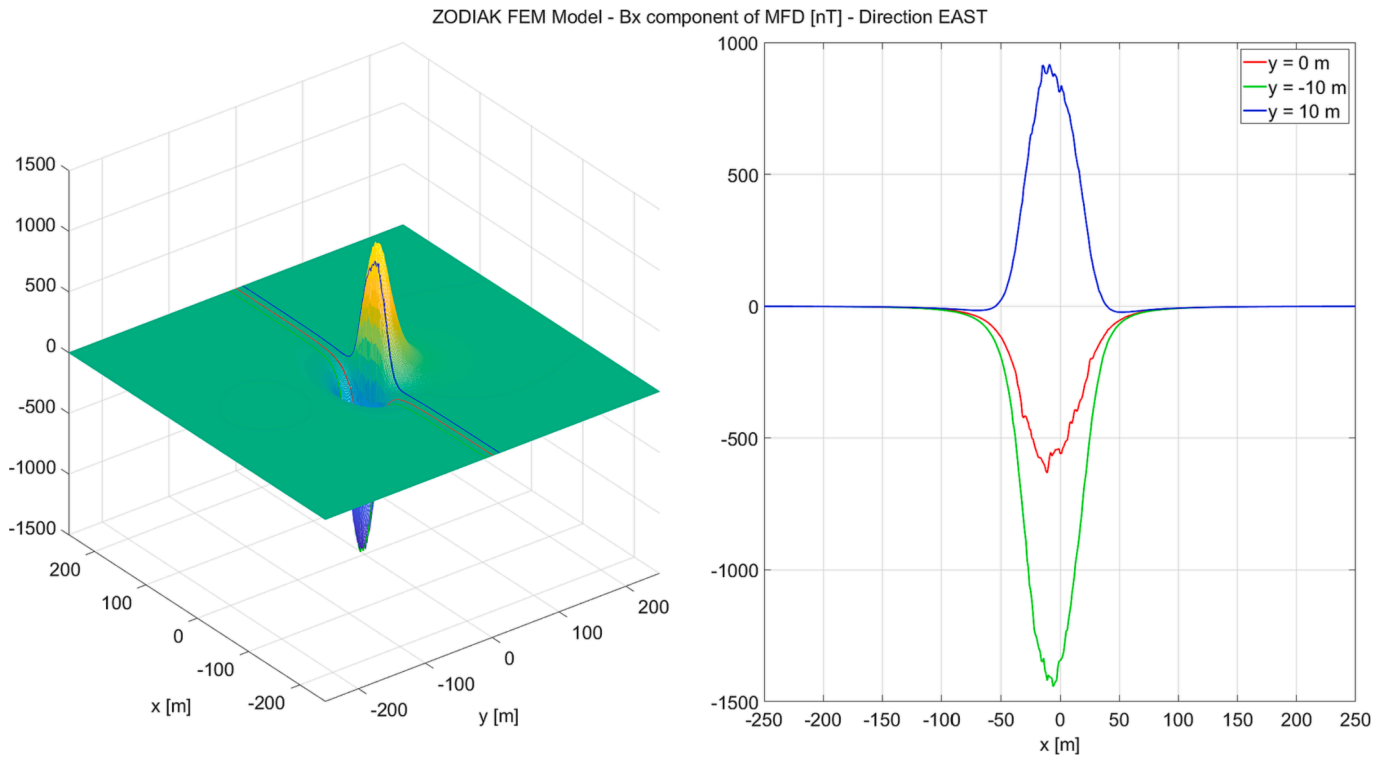

Fig. 35. The effect of the coordinate orthogonal to ship's motion on Bx component for east direction.

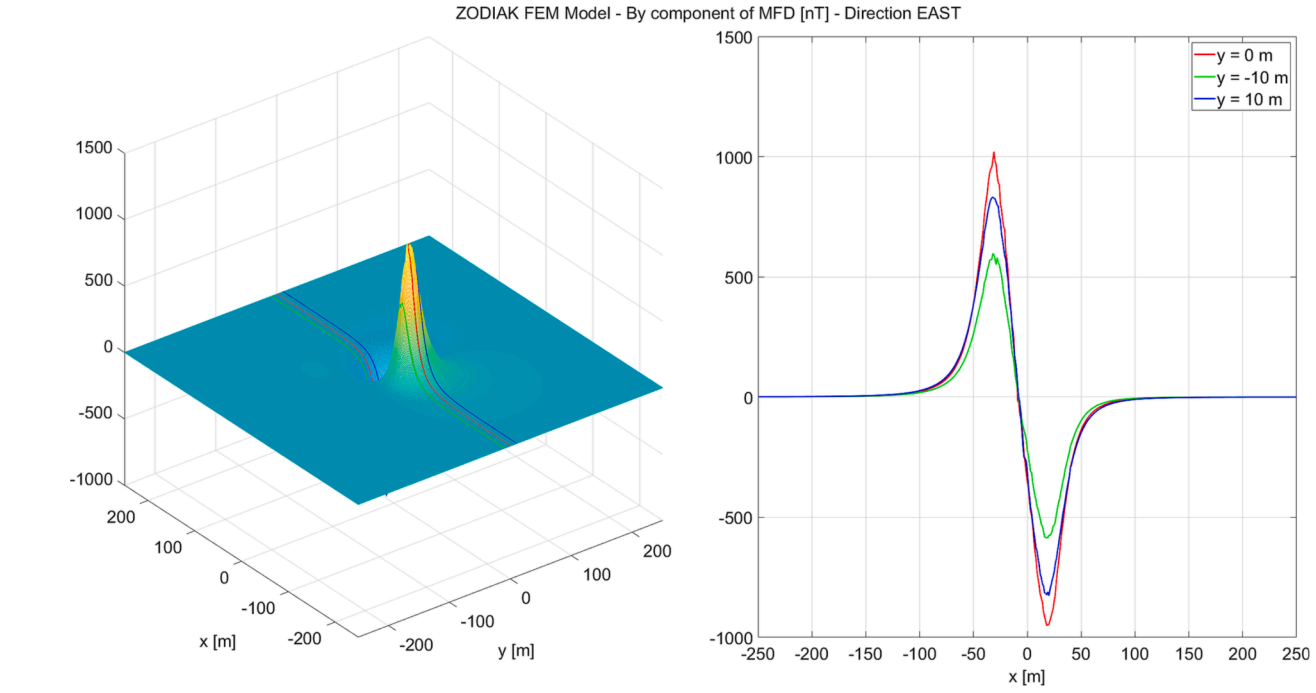

Fig. 36. The effect of the coordinate orthogonal to ship's motion on By component for east direction.

position, thus remaining stable at the specified geographic position.

During the tests conducted, a hybrid boat (RIB) was used (Fig. 37), which, although fast and maneuverable, is highly susceptible to environmental conditions when left stationary. This boat is not equipped with a thruster, and the only way to correct position is through the use of a propeller, which makes it difficult to stabilize its geographic position.

The underwater measurement module was lowered to the sea bottom from the bow of the boat using a hydraulic crane and a rope attached to a bracket at the top of the module. For this purpose, an additional pulley was used through which the rope was pulled. Once the module was set on bottom, the rope was picked out to the maximum, with the movement of the water and wind causing the boat to continuously drift and thus change its position relative to the module on the bottom. This situation is similar to the effects that occur when anchoring a vessel [35,36], i.e., wind, current, wave action, and the depth at which the anchor is located.

The movement of the boat relative to the module's anchorage

Fig. 37. Transporting the measurement module to the target geographic position using a hybrid boat.

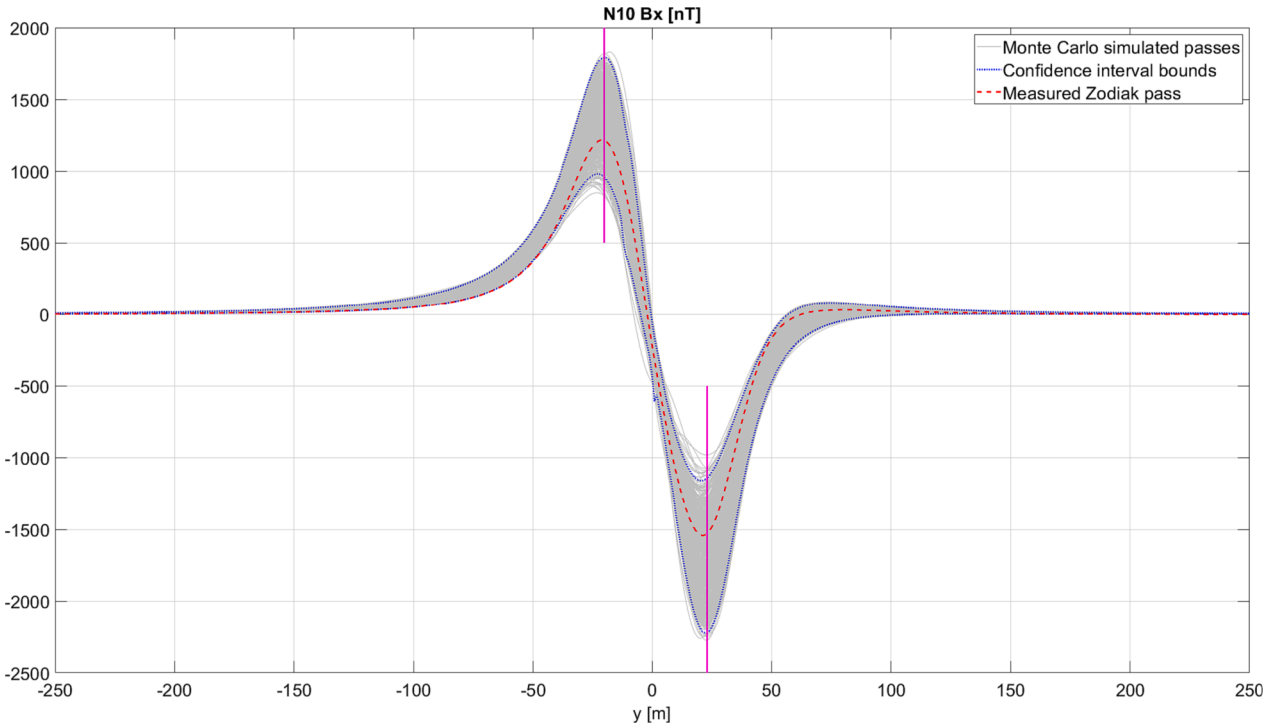

Fig. 38. Determining the confidence interval for N10 Bx.

introduced additional uncertainty in determining the geographic position. This uncertainty can reach up to 10 m, thus affecting the accuracy of subsequent measurements.

In order to model a simulation scenario that takes into account the described phenomenon of boat drift relative to the submerged measuring device, the approach to determining the offset was changed from that described previously to a uniform distribution within the limits (-10 m to + 10 m). The noise model was left unchanged. The applied approach allowed MC simulations with virtual ship transitions within a dozen meters of the recorded original routes.

4.7. *Determining confidence interval*

The Fig. 38 shows in gray the family of determined signatures for the N10 path and the B_x component using 1000 Monte Carlo simulations, taking into account the modeled ship position errors. At the point y = -20 the maximum signatures occur, and at the point y = 23 the minimum signatures occur. These are good places to inspect the distribution of these signatures.

Fig. 39 and Fig. 40 show the distributions at these points. Due to the asymmetric and irregular distributions of errors at the input used in the design of Monte Carlo simulations (resulting from measurements), the

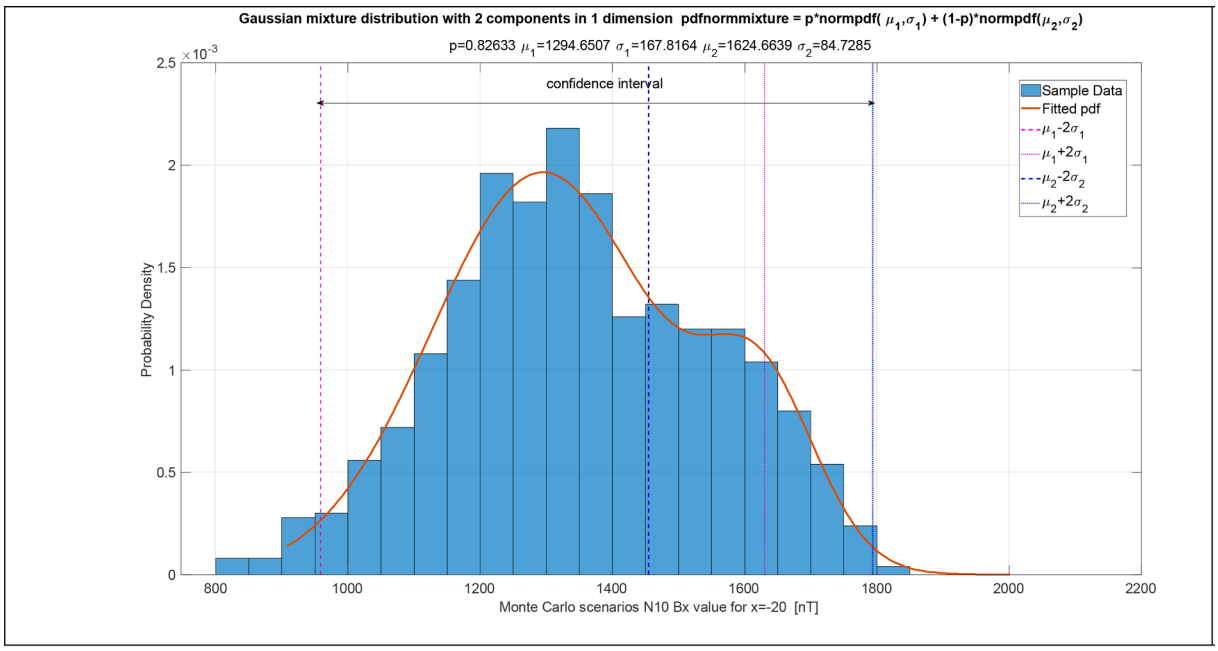

Fig. 39. Histogram and PDF approximation for N10 Bx(−20) - maximum signature values.

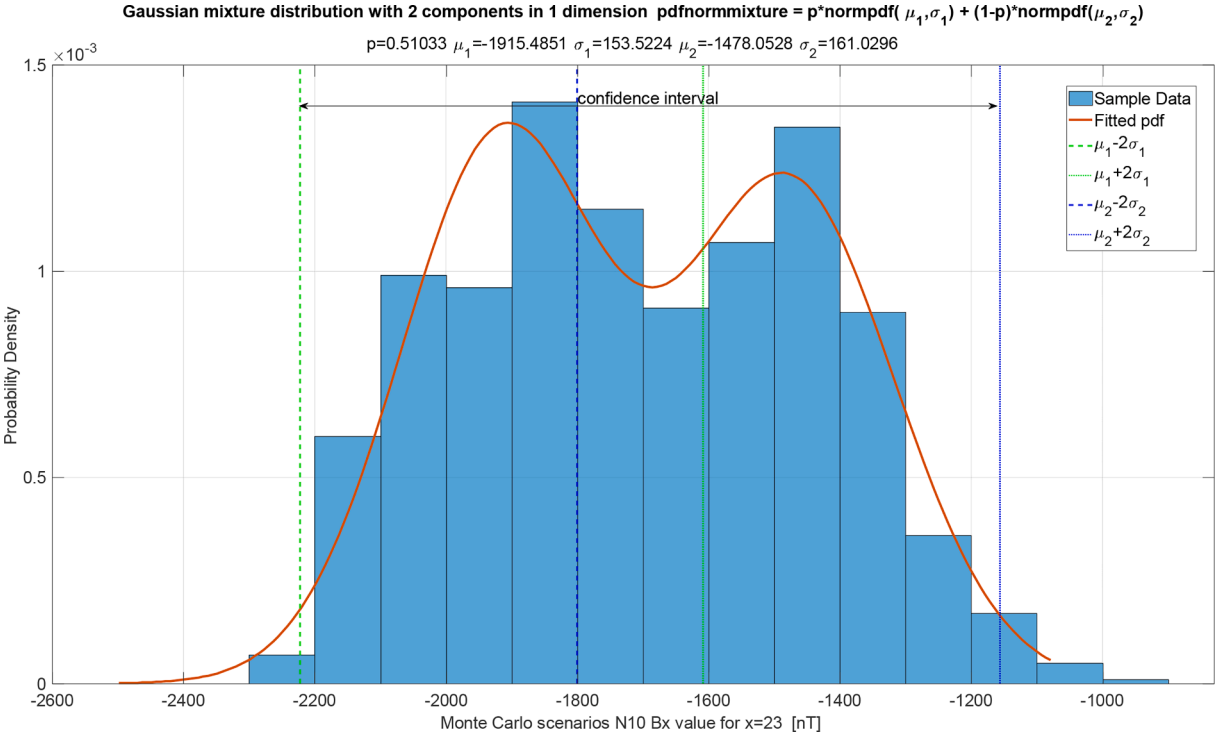

Fig. 40. Histogram and PDF approximation for N10 Bx(23) - minimum signature values.

simulation results are also not symmetrical and cannot be described by known classical distributions. Analyzing the distributions of signatures at many points, it was found that a good approximation of these distributions may be a composite of two Gaussian distributions. The results of these approximations with the values of the estimated parameters are presented in Fig. 39 and Fig. 40. When describing the confidence interval for a normal distribution, distances of 2*σ from the mean are used. Therefore, a lower bound of confidence interval was established as $CI_L = \min(\mu_1 - 2\sigma_1, \mu_2 - 2\sigma_2)$ and higher bound of confidence interval approach was established as $CI_H = \max(\mu_1 + 2\sigma_1, \mu_2 + 2\sigma_2)$. Using this method, confidence intervals were determined at each point of the characteristic, which were presented in the drawings (Fig. 41-43) for all the waveforms analyzed in the article.

A summary of the research conducted in the article is visually presented in Fig. 41-43 in the form of graphs. Quantitative indicators can also be useful for conducting performance analysis. Classic statistical indicators RMSE (Root Mean Square Error) and MAE (Mean Absolute Error) data were prepared according to formulas (15) and (16).

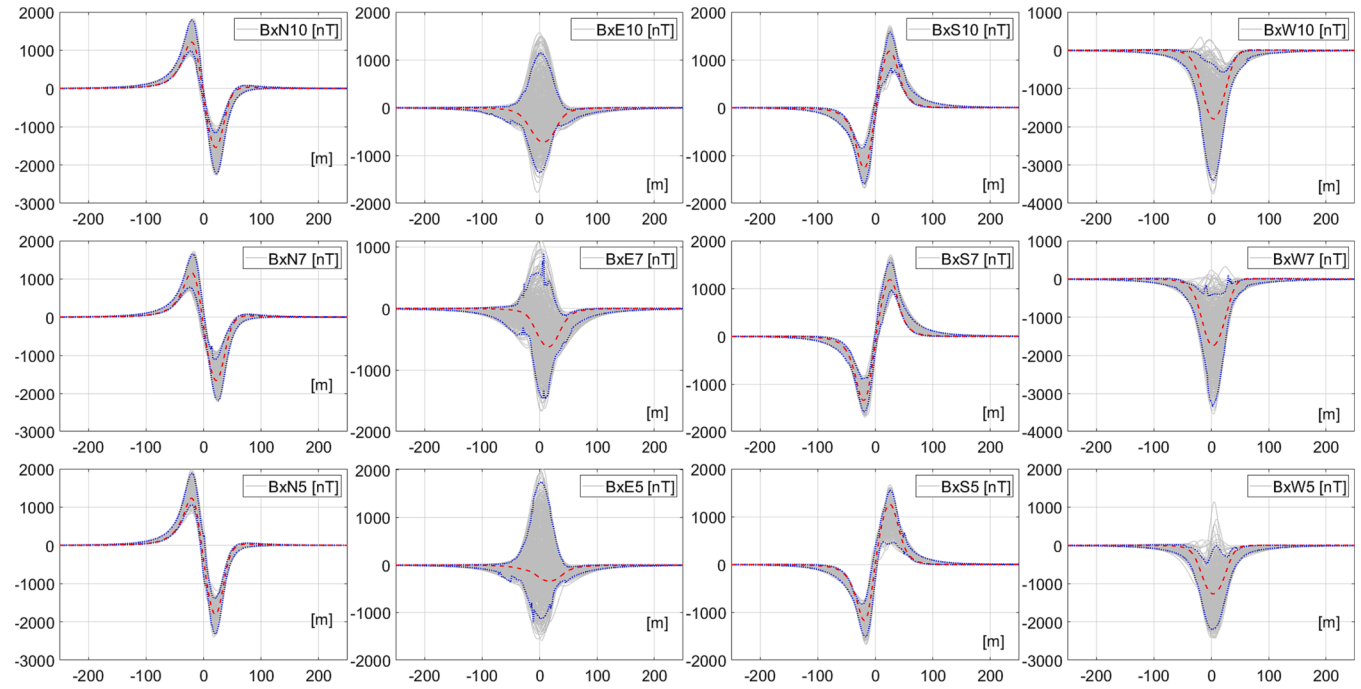

Fig. 41. Method B results - Bx component of MF (red – measured, grey - Monte Carlo simulations, blue – confidence interval). (For interpretation of the references to colour in this figure legend, the reader is referred to the web version of this article.)

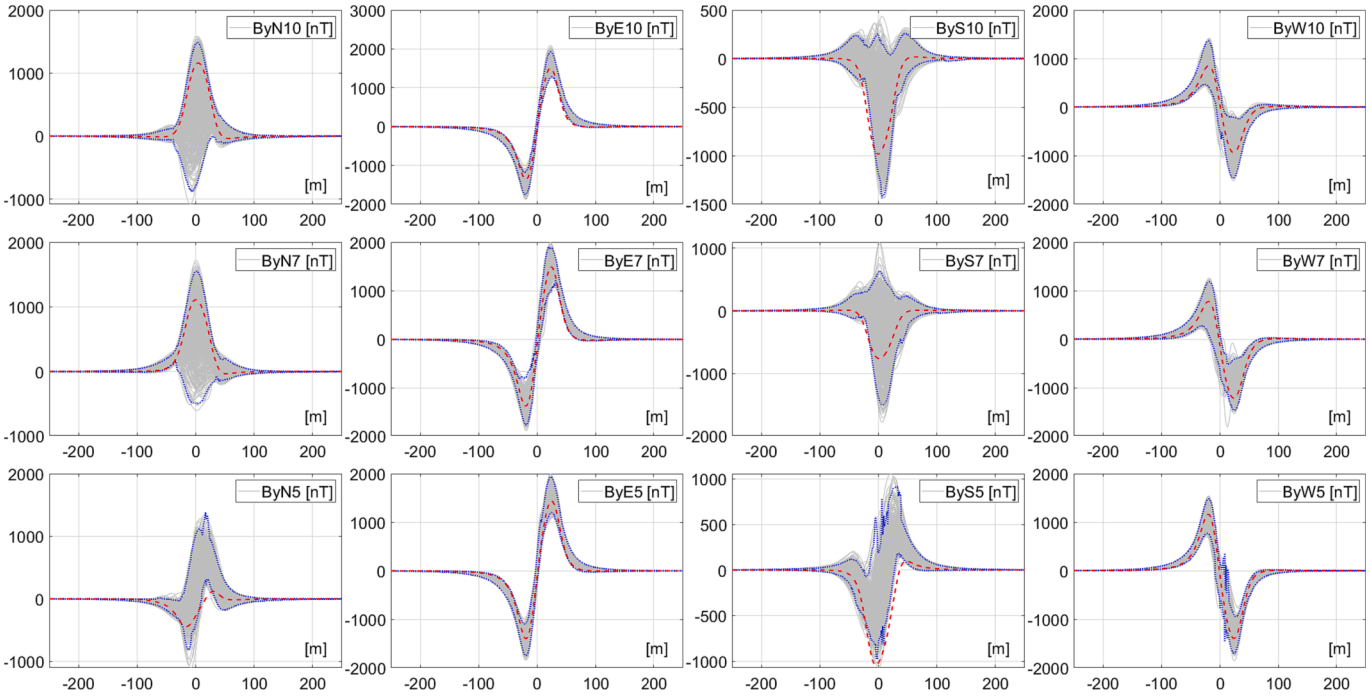

Fig. 42. Method B results - By component of MF (red – measured, grey - Monte Carlo simulations, blue – confidence interval). (For interpretation of the references to colour in this figure legend, the reader is referred to the web version of this article.)

$$RMSE = \sqrt{\frac{1}{N}\sum_{i=1}^{N}(ref_i - model_i)^2} \tag{15}$$

$$MAE = \frac{1}{N}\sum_{i=1}^{N}|ref_i - model_i| \tag{16}$$

where $model_i$ is the vector of N signature values at i-th position coordinate counted by the model, and ref_i is the vector of N reference signature values at the same position. Maximum and minimum values of RMSE and MAE are provided to the reader.

Another metric called "CI max span " given as (17) means the maximum spread between the upper and lower bounds of the confidence interval for all samples in the path. Its unit is nT and it has the dimension of maximum uncertainty for a given transition. The last indicator given as (18) is the "CI area" which is the area between the upper and lower bounds of the confidence interval along the entire path. The dimension of this field is expressed in the artificial unit nT·m and has the meaning

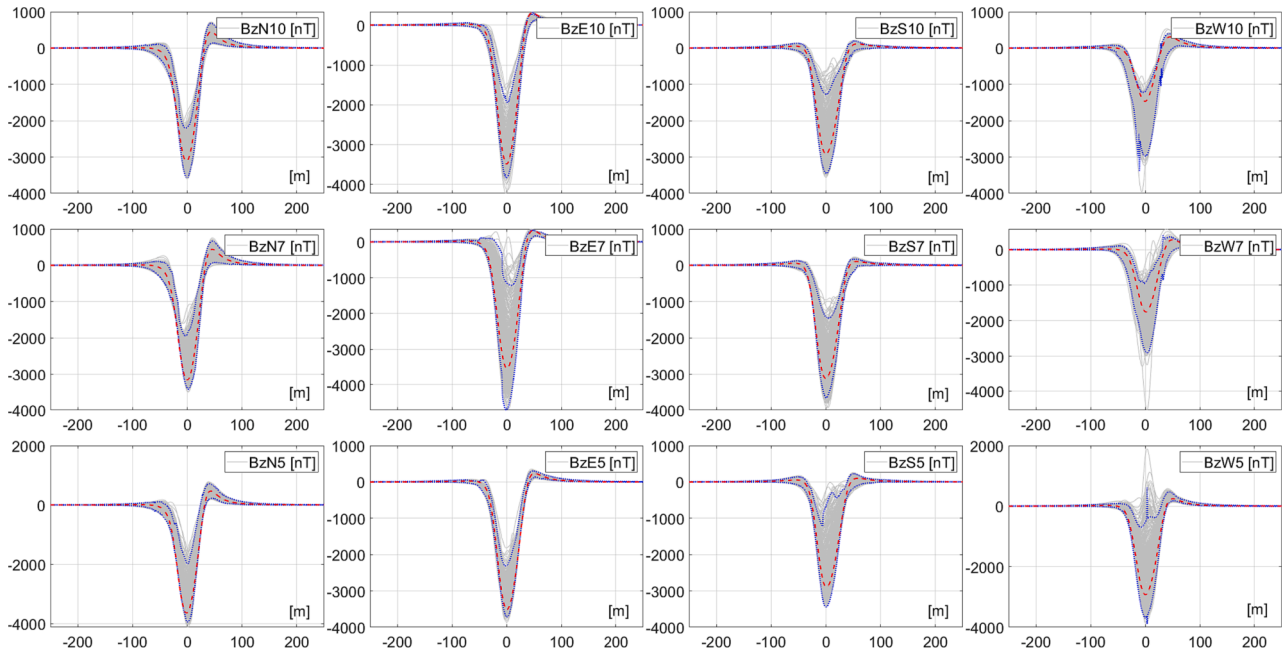

Fig. 43. Method B results - Bz component of MF (red – measured, grey - Monte Carlo simulations, blue – confidence interval). (For interpretation of the references to colour in this figure legend, the reader is referred to the web version of this article.)

Table 3
Quantitative indicators for Bx component of MF.

N10 Bx	E10 Bx	S10 Bx	W10 Bx
RMSE 81.6, 46.5 nT	RMSE 174.6, 108.1 nT	RMSE 61.2, 26.5 nT	RMSE 157.6, 93.6 nT
MAE 44.6, 24.3 nT	MAE 75.4, 36.0 nT	MAE 35.3, 15.8 nT	MAE 73.7, 40.8 nT
CI max span 1082.0 nT	CI max span 2494.4 nT	CI max span 817.4 nT	CI max span 3041.0 nT
CI area 82166.8 nT·m	CI area 149632.7 nT·m	CI area 79390.8 nT·m	CI area 173134.8 nT·m
N7 Bx	E7 Bx	S5 Bx	W7 Bx
RMSE 80.9, 42.1 nT	RMSE 96.2, 62.3 nT	RMSE 74.3, 30.7 nT	RMSE 141.5, 88.3 nT
MAE 41.8, 22.1 nT	MAE 48.5, 24.9 nT	MAE 38.7, 17.3 nT	MAE 66.1, 37.9 nT
CI max span 1194.8 nT	CI max span 2215.3 nT	CI max span 1111.3 nT	CI max span 2946.3 nT
CI area 88378.9 nT·m	CI area 134129.2 nT·m	CI area 85872.6 nT·m	CI area 162765.4 nT·m
N5 Bx	E5 Bx	S5 Bx	W5 Bx
RMSE 79.5,30.2 nT	RMSE 155.2, 118.9 nT	RMSE 74.3, 30.7 nT	RMSE 163.1, 52.8 nT
MAE 39.2,16.5 nT	MAE 66.3, 39.0 nT	MAE 38.7, 17.3 nT	MAE 83.0, 24.9 nT
CI max span 1150.1 nT	CI max span 2868.8 nT	CI max span 1111.3 nT	CI max span 2137.8 nT
CI area 80222.3 nT·m	CI area 166066.4 nT·m	CI area 85872.6 nT·m	CI area 132081.9 nT·m

Table 4
Quantitative indicators for By component of MF.

N10 By	E10 By	S10 By	W10 By
RMSE 144.1,92.1 nT	RMSE 90.4,30.8 nT	RMSE 163.0,51.4 nT	RMSE 97.8,33.9 nT
MAE 55.1,30.9 nT	MAE 52.6,20.6 nT	MAE 70.3,15.9 nT	MAE 49.5,18.7 nT
CI max span 2267.8 nT	CI max span 683.4 nT	CI max span 1597.6 nT	CI max span 1258.6 nT
CI area 120825.7 nT·m	CI area 70557.0 nT·m	CI area 96642.4 nT·m	CI area 100027.8 nT·m
N7 By	E7 By	S7 By	W7 By
RMSE 104.3,74.0 nT	RMSE 77.3,32.1 nT	RMSE 151.7,69.6 nT	RMSE 91.9,43.0 nT
MAE 42.9,25.6 nT	MAE 44.3,19.7 nT	MAE 64.8,23.5 nT	MAE 45.9,17.6 nT
CI max span 2050.0 nT	CI max span 1046.5 nT	CI max span 2099.7 nT	CI max span 1193.6 nT
CI area 113361.9 nT·m	CI area 89098.7 nT·m	CI area 122733.4 nT·m	CI area 100777.3 nT·m
N5 By	E5 By	S5 By	W5 By
RMSE 189.3,45.5 nT	RMSE 91.2,31.0 nT	RMSE 227.1,51.1 nT	RMSE 71.9,26.3 nT
MAE 75.9,15.0 nT	MAE 51.2,21.2 nT	MAE 94.6,18.9 nT	MAE 36.9,12.8 nT
CI max span 1435.6 nT	CI max span 753.8 nT	CI max span 1597.1 nT	CI max span 1819.2 nT
CI area 94882.5 nT·m	CI area 79803.6 nT·m	CI area 93127.5 nT·m	CI area 84176.7 nT·m

of the total amount of uncertainty.

$$\text{CI max span} = \max_{x\in(-250,250)} (CI_H(x) - CI_L(x)) \tag{17}$$

$$\text{CI area} = \int_{x=-250}^{250} CI_H(x) - CI_L(x)dx \tag{18}$$

where $CI_H(x)$ is the value of upper bound of confidential interval and $CI_L(x)$ is the value of lower bound of confidential interval at point x.

Quantitative indicators are collected in Tables 3-5 organized in order compatible with Fig. 41-43 for ease of evaluation.

Analyzing the results presented in Fig. 41-43 and Tables 3-5, it can be concluded that, collectively, the MC-type simulation well modelled the conditions in which the family of signature waveforms coincided with the recorded magnetic field measurements. Better results were obtained with extended method than with basic method, but the width of the signature waveform intervals increased significantly. The course of ship's position changes can possibly be explained by pure randomness, but then the ranges in which the signatures are found are significantly wider.

5. Conclusions

In 2019, a measurement campaign was carried out by recording

Table 5
Quantitative indicators for Bz component of MF.

N10 Bz	E10 Bz	S10 Bz	W10 Bz
RMSE	RMSE 102.4,67.2	RMSE	RMSE 164.0,90.4
100.0,45.0 nT	nT	128.9,101.7 nT	nT
MAE 48.3,19.2	MAE 44.0,22.3	MAE 53.8,35.1	MAE 67.0,31.5
nT	nT	nT	nT
CI max span	CI max span	CI max span	CI max span
1395.6 nT	1973.7 nT	2171.7 nT	2305.1 nT
CI area 109075.3	CI area 108926.2	CI area 125526.9	CI area 123733.7
nT·m	nT·m	nT·m	nT·m
N7 Bz	E7 Bz	S7 Bz	W7 Bz
RMSE	RMSE	RMSE	RMSE 119.0,60.6
142.3,68.8 nT	154.6,137.8 nT	138.1,101.6 nT	nT
MAE 63.6,25.2	MAE 60.9,46.9	MAE 54.8,36.9	MAE 49.2,22.0
nT	nT	nT	nT
CI max span	CI max span	CI max span	CI max span
1736.7 nT	3591.9 nT	2235.0 nT	2132.3 nT
CI area 122240.7	CI area 178077.8	CI area 124651.6	CI area 130698.8
nT·m	nT·m	nT·m	nT·m
N5 Bz	E5 Bz	S5 Bz	W5 Bz
RMSE	RMSE 96.4,64.1	RMSE	RMSE
151.6,93.3 nT	nT	133.3,115.2 nT	243.2,150.8 nT
MAE 65.6,34.8	MAE 40.4,21.7	MAE 55.1,39.9	MAE 92.7,54.7
nT	nT	nT	nT
CI max span	CI max span	CI max span	CI max span
2074.6 nT	1445.5 nT	2892.0 nT	4499.3 nT
CI area 136459.8	CI area 87951.1	CI area 141374.4	CI area 161724.5
nT·m	nT·m	nT·m	nT·m

magnetic flux density values at ship's transits in four cardinal geographic directions. The geographic positions of the ship and the measuring device were determined using a GPS receiver of a typical class for ships of this type and being their standard equipment. The data on the ship's position relative to the measuring device, along with the ship heading and magnetic flux density, were entered into a multi-dipole model which was then used to determine the magnetic signatures. Comparing the experimentally recorded ship positions relative to the measuring device and the determined signatures with the corresponding synthetic data has revealed a discrepancy in the results obtained in this way. The performed analysis of the influence of errors from the magnetometers has proven that these errors could not deform the magnetic signatures to such a large extent. Therefore, an assumption has been made that another very possible source of errors having a great impact on the anomalies in the signatures is the inaccuracies in determining the position of the measuring device and the ship.

That is why in 2021, a new measurement campaign was carried out, which was intended to assess the level of errors in determining the position of a ship in motion. The measurements were made on the same measurement ground and using the same GPS receiver as that used during the first measurement campaign, along with another receiver as a reference. The obtained results allowed to assess the error as amounting to several meters. In addition, in 2021, both of these receivers were placed in the vicinity of the measurement ground to assess the error in determining the geographic position in static conditions, in the absence of movement. Also in this case, an error of several meters for 'virtual' ship position change during several hours of measurement was obtained. Thus, empirical confirmation was obtained that the 2019 measurements could have been burdened with a significant error in determining the relative position between the measuring device and the passing ship. A statistical analysis of this errors was performed by constructing its distributions.

The obtained error distributions in determining the geographic position were used to build random black-box error models for position determining of the ship and the measuring device. Two different approaches to error modeling were used: a model resulting from differences between GPS receiver readings, and a model based on possible drift of the measuring device. The error models were superimposed on the originally determined ship's routes, thus creating a virtual passage of the ship relative to the measuring device which represented a possible real route of the ship during the measurements. In accordance with the idea of Monte Carlo simulation, not only one model was developed, but the experiment was repeated many times. With each possible route, a new form of magnetic signatures was determined based on the originally recorded values of magnetic flux density and the currently determined route of the ship's transitions and headings.

The result of these experiments is a family of signatures that represents possible values of the signatures taking into account the uncertainty in determining the position of the ship and the measuring device, as modelled by statistical error distributions. The analysis of the obtained results has indicated that the nature of the signatures could be significantly different for a ship position difference of several meters, which confirms the results of previous studies. The approach taking into account a possible drift of the measuring device during the measurement campaign has shown that the signatures recorded in 2019 are included in the plotted sets of possible signatures, which is in line with the previous guesses and confirms the usefulness of the presented approach.

The basic observation is that the accuracy in determining geographic position has a significant impact on the quality of the magnetic signatures obtained. Analyzing the waveforms of individual simulation scenarios, one can see how the impact of an error of a few meters completely changes the nature of the signature. The performed simulations have confirmed that the results considered in earlier studies were subject to errors originating from faulty determination of ship's geographic position relative to the measuring device.

Eliminating the impact of positioning inaccuracy is difficult to achieve for typical commercial vessels using satellite navigation systems, in accordance with SOLAS (International Convention for the Safety of Life at Sea). The accuracy of the systems used is sufficient from the point of view of the safe movement of the vessel from source port to destination port.

A possible solution to the problem would be to install a portable reference system, e.g. Leica GS18T, onboard for the duration of the magnetic field measurements at the designated measuring range. However, it should be borne in mind that the high accuracy of this system (RTK) requires stable mobile phone coverage (corrections from reference stations are sent via GPRS), i.e. in practice a distance from shore no further than LOS (Line of Sight).

Eliminating the impact of inaccuracy in determining the position of the underwater measurement system could be achieved with an additional active acoustic positioning system. This solution requires additional resources, both on the underwater measurement module and the survey vessel. A limited budget was available for the survey campaign carried out. The indicated solution should be taken into account when planning future magnetic signature measurements of ships.

Finally, it can be concluded that even with a campaign conducted with an error-prone GPS device, it is possible with the above presented analysis to show the signature range within which the actual signature should be.

CRediT authorship contribution statement

J. Tarnawski: Writing – review & editing, Writing – original draft, Visualization, Supervision, Software, Project administration, Methodology, Investigation, Conceptualization. **K. Buszman:** Writing – review & editing, Writing – original draft, Resources, Methodology, Investigation, Data curation. **M. Woloszyn:** Writing – review & editing, Methodology, Formal analysis, Conceptualization. **B. Puchalski:** Investigation, Conceptualization.

Declaration of competing interest

The authors declare that they have no known competing financial interests or personal relationships that could have appeared to influence the work reported in this paper.

Data availability

Data will be made available on request.

References

[1] Satellite Compas Furuno SC-50 technical documentation, SC50, (2021). https://www.furunousa.com/en/support/SC50.

[2] Statki Urzedu Morskiego w Gdyni, Statki Urzedu Morskiego w Gdyni - Zodiak (in Polish), Statki Urzedu Morskiego w Gdyni. (2021). https://bazagdansk.pl/index.php?news&nid=35 (accessed June 5, 2021).

[3] Polski Rejestr Statków S. A. (PRS), Register Of Ships 2021, Register Of Sea-Going Ships 2021. (2021) 1–190. https://www.prs.pl/wydawnictwa/rejestry-statkow-jachtow-lodzi.

[4] I. Gloza, K. Buszman, The multi-influence passive module for underwater environment monitoring, Hydroacoustics. 14 (2011) (accessed August 10, 2023), http://pta.eti.pg.gda.pl/journal/paper.py?id=497.

[5] J. Tarnawski, K. Buszman, M. Woloszyn, T.A. Rutkowski, A. Cichocki, R. Józwiak, Measurement campaign and mathematical model construction for the ship *zodiak* magnetic signature reproduction, Measurement 186 (2021) 110059, https://doi.org/10.1016/j.measurement.2021.110059.

[6] J. Tarnawski, T. Rutkowski, M. Woloszyn, A. Cichocki, K. Buszman, Magnetic signature description of ellipsoid-shape vessel using 3D multi-dipole model fitted on cardinal directions, IEEE Access 10 (2022) 1, https://doi.org/10.1109/ACCESS.2022.3147138.

[7] A. Oxley, Uncertainties in GPS positioning: a mathematical discourse, 1st ed., Academic Press, 2017 https://www.elsevier.com/books/uncertainties-in-gps-positioning/oxley/978-0-12-809594-2.

[8] F. Rovira-Más, Vulnerability of GPS to provide vehicle states in real time, IFAC Proceedings Volumes (IFAC-PapersOnline) IFAC Secretariat (2013) 207–212, https://doi.org/10.3182/20130828-2-SF-3019.00002.

[9] S.P. Mertikas, DISTRIBUTIONS ERROR, AND ACCURACY MEASURES, IN NAVIGATION: AN OVERVIEW, 1985.

[10] D.Y. Hsu, Spatial error analysis: a unified application-oriented treatment, 1st edition, Wiley-IEEE Press, New York, 1998.

[11] A. Banachowicz, R. Bober, A. Wolski, G. Banachowicz, Spatial accuracy of GPS/DGPS positions in a fairway, Reports on Geodesy. Z. 2 (73) (2005) 337–341.

[12] R. Bober, T. Szewczuk, A. Wolski, Effect of measurement duration on the accuracy of position determination in GPS and GPS/EGNOS systems, TransNav : Int. J. Marine Navigation and Safety of Sea Trans. 4 (2010) (accessed August 10, 2023), http://yadda.icm.edu.pl/baztech/element/bwmeta1.element.baztech-5ec25197-79cd-4252-8055-bd03169a00a4.

[13] J. Tarnawski, A. Cichocki, T.A. Rutkowski, K. Buszman, M. Woloszyn, Improving the quality of magnetic signature reproduction by increasing flexibility of multi-dipole model structure and enriching measurement information, IEEE Access 8 (2020) 190448–190462, https://doi.org/10.1109/ACCESS.2020.3031740.

[14] W. Chen, C. Xiong, L. Yu, S. Lian, Z. Ye, Dynamic monitoring of an offshore jacket platform based on RTK-GNSS measurement by CF-CEEMDAN method, Appl. Ocean Res. 115 (2021) 102844, https://doi.org/10.1016/j.apor.2021.102844.

[15] X. Xue, H. Qin, H. Lu, High-precision time synchronization of kinematic navigation system using GNSS RTK differential carrier phase time transfer, Measurement 176 (2021) 109132, https://doi.org/10.1016/j.measurement.2021.109132.

[16] GPS receiver Leica GS18T technical documentation, 'Leica_GS18_T_DS,' (2021). https://leica-geosystems.com/-/media/files/leicageosystems/products/datasheets/leica_gs18_t_ds.ashx?la=en&hash=63C4FF25035B5C81FF0E00776E300705.

[17] GPS controller Leica CS20 technical documentation, (2021). https://leica-geosystems.com/-/media/files/leicageosystems/products/datasheets/leica_captivate_cs20_ds_1119_en.ashx?la=en&hash=2B9414E1DACF426157DD662A6C5C169A.

[18] SmartNet system description, (2021). https://hxgnsmartnet.com/en-gb/howit-works.

[19] SmartNet Reference station map, 2021. https://www.smartnetleica.pl/smartnet/zasoby/mapa-stacji-referencyjnych/.

[20] A. Seijmonsbergen, The modern geomorphological map, Treatise on Geomorphology (2013) 35–52, https://doi.org/10.1016/B978-0-12-374739-6.00371-7.

[21] H. Oda, E. Okuyama, E. Shimizu, Ship to ship operations monitoring system using high accuracy DGPS, IFAC Proceedings Volumes (IFAC-PapersOnline), IFAC Secretariat (2010) 62–66, https://doi.org/10.3182/20100915-3-DE-3008.00021.

[22] A. Banachowicz, R. Bober, T. Szewczuk, A. Wolski, Monitoring of cargo transport in urban areas using GPS/EGNOS technologies as part of the safety system, Procedia. Soc. Behav. Sci. 151 (2014) 371–380, https://doi.org/10.1016/j.sbspro.2015.05.100.

[23] J. Benedicto, P. Michel, J. Ventura-Traveset, EGNOS: project status overview, Air Space Eur. 1 (1999) 58–64, https://doi.org/10.1016/S1290-0958(99)80041-0.

[24] C. Adrados, I. Girard, J.P. Gendner, G. Janeau, Global positioning system (GPS) location accuracy improvement due to selective availability removal, Comptes Rendus - Biologies. 325 (2002) 165–170, https://doi.org/10.1016/S1631-0691(02)01414-2.

[25] B.D. Flury, Acceptance-rejection sampling made easy, SIAM Rev. 32 (1990) 474–476, https://doi.org/10.1137/1032082.

[26] A.F.M. Smith, G.O. Roberts, Bayesian computation via the gibbs sampler and related markov chain monte carlo methods, J. Roy. Stat. Soc.: Ser. B (Methodol.) 55 (1993) 3–23, https://doi.org/10.1111/j.2517-6161.1993.tb01466.x.

[27] B. Ripley, Stochastic Simulation, in: Stochastic Simulation, John Wiley & Sons, Ltd, 1987: pp. i–xi 10.1002/9780470316726.fmatter.

[28] Stochastic Modelling and Applied Probability, Springer. (n.d.). https://www.springer.com/series/602 (accessed September 2, 2023).

[29] C. Graham, D. Talay, Stochastic simulation and monte carlo methods: mathematical foundations of stochastic simulation, springer, Berlin, Heidelberg (2013), https://doi.org/10.1007/978-3-642-39363-1.

[30] R.L. Harrison, Introduction to monte carlo simulation, AIP Conference Proceedings 1204 (2010) 17–21, https://doi.org/10.1063/1.3295638.

[31] D. van Ravenzwaaij, P. Cassey, S.D. Brown, A simple introduction to markov chain monte-carlo sampling, Psychon Bull Rev. 25 (2018) 143–154, https://doi.org/10.3758/s13423-016-1015-8.

[32] N. Metropolis, A.W. Rosenbluth, M.N. Rosenbluth, A.H. Teller, E. Teller, Equation of state calculations by fast computing machines, J. Chem. Phys. 21 (1953) 1087–1092, https://doi.org/10.1063/1.1699114.

[33] G.O. Roberts, J.S. Rosenthal, Examples of adaptive MCMC, J. Comput. Graph. Stat. 18 (2009) 349–367, https://doi.org/10.1198/jcgs.2009.06134.

[34] W.K. Hastings, Monte Carlo sampling methods using markov chains and their applications, Biometrika 57 (1970) 97–109, https://doi.org/10.2307/2334940.

[35] Adam Kowalski, Safety problems of anchoring in restricted areas in extreme hydrometeorological conditions, 45 Scientific Journals of the Maritime University of Szczecin. 117 (2016) 120 125 10.17402/095.

[36] A. Nowicki, Wiedza o manewrowaniu statkami morskimi, Księgarnia Oficyna Morska. (1999). https://sklep.oficynamorska.pl/pl/p/Wiedza-o-manewrowaniu-statkami-morskimi/174 (accessed September 2, 2023).

[37] M. Woloszyn, J. Tarnawski, J. Woloszyn, Decomposition of the induced magnetism degaussing problem for fast determination of currents in demagnetization coils wrapped outside an object under arbitrary external field conditions, J. Magn. Magn. Mater. 580 (2023) 170898, https://doi.org/10.1016/j.jmmm.2023.170898.

[38] M. Woloszyn, J. Tarnawski, Magnetic signature reproduction of ferromagnetic ships at arbitrary geographical position, direction and depth using a multi-dipole model, Sci Rep. 13 (2023) 14601, https://doi.org/10.1038/s41598-023-41702-4.

[39] Evaluation of Measurement Data—Supplement 1 to the Guide to the Expression Of Uncertainty in Measurement—Propagation of Distributions Using a Monte Carlo method, Standard JCGM 101:2008, International Organization for Standardization, Geneva, Switzerland, 2008.

[40] Cox M. G., Harris P. M., Software Support for Metrology Best Practice Guide No. 6, Uncertainty Evaluation, 2010.

[41] La. Marca, Paola, et al., Numerical and experimental estimation of measurement uncertainty in magnetic field mapping, IEEE Trans. Instrum. Meas. 71 (2022) 1–10.

[42] Y. Liu, B. Ravelo, A.K. Jastrzebski, Time-domain magnetic dipole model of PCB near-field emission, IEEE Trans. Electromagn. Compat. 58 (5) (2016) 1561–1569.